Nonlinear gravitational recoil from the mergers of precessing black-hole binaries

Carlos O. Lousto and Yosef Zlochower

Phys. Rev. D **87**, 084027 — Published 10 April 2013

DOI: 10.1103/PhysRevD.87.084027

Nonlinear Gravitational Recoil from the Mergers of Precessing Black-Hole Binaries

Carlos O. Lousto and Yosef Zlochower
Center for Computational Relativity and Gravitation, and School of Mathematical Sciences, Rochester Institute of Technology, 85 Lomb Memorial Drive, Rochester, New York 14623

We present results from an extensive study of 88 precessing, equal-mass black-hole binaries with large spins (83 with intrinsic spins $|\vec{S}_i/m_i^2|$ of 0.8 and 5 with intrinsic spins of 0.9), and use these data to model new nonlinear contributions to the gravitational recoil imparted to the merged black hole. We find a new effect, the *cross kick*, that enhances the recoil for partially aligned binaries beyond the *hangup kick* effect. This has the consequence of increasing the probabilities of recoils larger than 2000 km s^{-1} by nearly a factor two, and, consequently, of black holes getting ejected from galaxies and globular clusters, as well as the observation of large differential redshifts/blueshifts in the cores of recently merged galaxies.

PACS numbers: 04.25.dg, 04.30.Db, 04.25.Nx, 04.70.Bw

I. INTRODUCTION

The studies of black-hole binaries (BHBs) that immediately followed the 2005 breakthroughs in numerical relativity [1–3] soon revealed the importance of spin to the orbital dynamics [4]. One of the most striking result was the unexpectedly large recoil velocity imparted to the remnant due to an intense burst of gravitational radiation around merger [5, 6]. Recoil velocities as large as 4000 km s^{-1} were predicted for maximally spinning black holes [7] (in a configuration with both spins lying in the orbital plane, known as the *superkick* configuration). This prediction, which was based on model for the recoil velocities that was linear in the individual spins of the merging holes [5, 8], triggered several astronomical searches for recoiling supermassive black holes as the byproduct of galaxy collisions, producing several dozen potential candidates [9–17]. See Ref. [18] for a review.

Accretion effects [19, 20] would tend to align the spins of the BHs with the orbital angular momentum, suppressing the *superkick* and, apparently, the likelihood of observing large recoils. We recently found [21, 22] however, that there are nonlinear spin couplings that lead to even larger recoil velocities when the spins are partially aligned with the orbital angular momentum. These so called *hangup kick* recoils can be as large as 5000 km s^{-1} (see Fig. 1).

In this paper we continue our exploration of unexpectedly large nonlinear contributions to the net recoil [21, 22]. Here we concentrate on equal-mass BHBs that precess. Our ultimate goal is to derive an empirical formula that takes into account all major contributions to the recoil (at least to the level of a few percent accuracy). This would be a near hopeless task if we just start with a set of random configurations. Rather, we propose a program for developing sets of configurations with exact or approximate symmetries that allow us to model the recoil term by term. For example, in the *hangup kick* configurations [21, 22], the BHBs can be described by two parameters, the z component of the total spin S_z, and the in-plane component of $\vec{\Delta}$ ($\vec{\Delta} \propto \vec{S}_2 - \vec{S}_1$ in the equal-mass case). If the generic recoil is also a function of Δ_z, those terms would be suppressed in the *hangup kick* configurations. Here we continue the exploration by evolving configurations that activate different possible terms for the recoil.

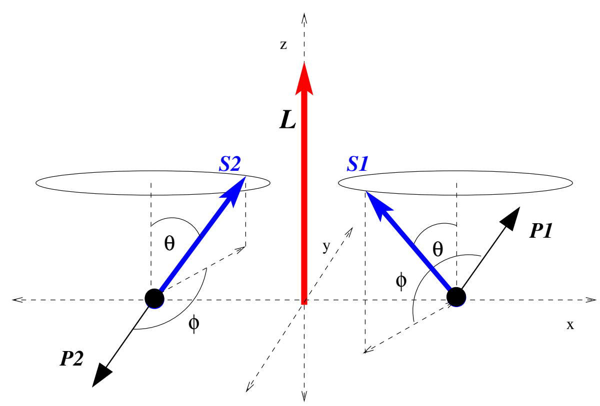

FIG. 1: The *hangup kick* configuration. Here $S_{1z} = S_{2z}$, while $S_{1x} = -S_{2x}$ and $S_{1y} = -S_{2y}$. The *hangup kick* configurations are preserved exactly by numerical evolutions.

Not all nonlinear terms in the spins lead to large increases in the recoil [23, 24]. We therefore need to perform many diverse simulations to try to elucidate which nonlinear terms contribute significantly and which can still be ignored. Here we explore the effects of precession on recoils. We perform simulations of equal-mass, precessing BHBs, but also discuss the more general unequal-mass case. We also extend the phenomenological formulas for predicting recoils to include higher powers of the spins, explicitly including up to fourth order, making use of discrete symmetry properties of the BHBs.

II. HIGHER ORDER RECOIL VELOCITY EXPANSIONS

Our approach to the modeling of recoil velocities of merged black holes is based on the numerical evidence that the vast majority of the recoil is produced by the anisotropic emission of gravitational radiation at the very last stage of the merger, i.e., when a common horizon forms (see, e.g., Fig 4 below). In order to model the dependence of the recoil on the spins of the individual holes (and the BHB's mass ratio), we were guided by the leading-order post-Newtonian (PN) expressions for the instantaneous radiated linear momentum [25] (higher-order PN couplings can be found in [26]). As such, we will use the typical PN variables, individual BH masses m_1 and m_2, total mass $m = m_1 + m_2$, mass difference $\delta m = (m_1 - m_2)/m$, mass ratio $q = m_1/m_2$, symmetric mass ratio $\eta = q/(1+q)^2$, total spin $\vec{S} = \vec{S}_1 + \vec{S}_2$, and $\vec{\Delta} = m(\vec{S}_2/m_2 - \vec{S}_1/m_1)$ (where $\vec{S}_i$ is the spin of BH i). For convenience, we also define dimensionless spin parameters $\vec{\alpha}_i = \vec{S}_i/m_i^2$. In terms of $\vec{\alpha}_i$, $\vec{S}$ and $\vec{\Delta}$ are given by $\vec{S} = m^2(\vec{\alpha}_2 + q^2\vec{\alpha}_1)/(1+q)^2$ and $\vec{\Delta} = m^2(\vec{\alpha}_2 - q\vec{\alpha}_1)/(1+q)$. Of particular importance here will be the components of $\vec{S}$ and $\vec{\Delta}$ along the direction of angular momentum $\hat{L}$, which we denote by with the subscript $\|$, and the projection of the vector into the plane orthogonal to $\hat{L}$, which we denote by a subscript $\perp$. Thus any vector can be written as $\vec{V} = \vec{V}_\| + \vec{V}_\perp$, where $\vec{V}_\| = (\hat{L}\cdot\vec{V})\hat{L}$ and $\vec{V}_\perp = \vec{V} - \vec{V}_\|$.

Although the PN approximation is not valid at the moment of the merger (PN theory does not even account for horizons), our ansatz is that the parameter dependence in these PN expressions yields a useful starting point for constructing empirical formulas for the recoil. Thus a PN expression of the form $\vec{F}(\vec{r},\vec{P})\cdot\vec{\Delta}$, where $\vec{F}$ is vector in the orbital plane, becomes a fitting term on our formula of the form $A\Delta_\perp\cos(\phi)$, where ϕ is the angle between $\vec{\Delta}_\perp$ and some weighted *averaged* direction of $\vec{F}$, and A is a fitting constant. However, in general, we do not know the weighted *averaged* direction of $\vec{F}$ and instead measure the angle ϕ with respect to a fiducial direction $\hat{n}$ (typically we chose $\hat{n} = \hat{r}_1 - \hat{r}_2$, the direction from BH2 to BH1) and add an angular fitting constant ϕ_0 to the formula, i.e. $A\Delta_\perp\cos(\phi - \phi_0)$ (the value of ϕ_0 obtained from the fit then gives the relative orientation between our fiducial $\hat{n}$ and the weighted *averaged* direction of $\vec{F}$).

We then verify that such PN-inspired formulas are accurate *a posteriori* by comparing our predictions to recoil results from other simulations. This is the basis of our phenomenological approach to modeling of recoil velocities and can be summarized in an expression for the three components of the velocity linear in the individual spins of the holes [5, 7, 27]

$$\vec{V}_{\rm recoil}(q,\vec{\alpha}) = V_m\,\hat{e}_1 + V_\perp(\cos\xi\,\hat{e}_1 + \sin\xi\,\hat{e}_2) + V_\|\,\hat{L}, \quad (1)$$

where

$$\begin{aligned}
V_m &= A_m\frac{\eta^2(1-q)}{(1+q)}\left[1 + B_m\,\eta\right],\\
V_\perp &= H\frac{\eta^2}{(1+q)}\Big[(1+B_H\,\eta)\,(\alpha_2^\| - q\alpha_1^\|)\\
&\quad + H_S\,\frac{(1-q)}{(1+q)^2}\,(\alpha_2^\| + q^2\alpha_1^\|)\Big],\\
V_\| &= K\frac{\eta^2}{(1+q)}\Big[(1+B_K\,\eta)\left|\vec{\alpha}_2^\perp - q\vec{\alpha}_1^\perp\right|\\
&\quad \times\cos(\phi_\Delta - \phi_1)\\
&\quad + K_S\,\frac{(1-q)}{(1+q)^2}\,\left|\vec{\alpha}_2^\perp + q^2\vec{\alpha}_1^\perp\right|\\
&\quad \times\cos(\phi_S - \phi_2)\Big],
\end{aligned} \quad (2)$$

$\hat{e}_1, \hat{e}_2$ are orthogonal unit vectors in the orbital plane, and ξ measures the angle between the unequal mass and spin contribution to the recoil velocity in the orbital plane. The angles ϕ_Δ and ϕ_S are defined as the angle between the in-plane component $\vec{\Delta}_\perp$ and $\vec{S}_\perp$ respectively and a fiducial direction at merger (see Ref. [28] for a description of the technique). Phases ϕ_1 and ϕ_2 depend on the initial separation of the holes for quasicircular orbits (astrophysically realistic evolutions of comparable masses BHs lead to nearly zero eccentricity mergers).

Note that the expression for V_m was determined in [29, 30]. The current estimates for the above parameters are[28, 29, 31] : $A_m = 1.2\times10^4\ {\rm km\,s^{-1}}$, $B_m = -0.93$, $H = (6.9\pm0.5)\times10^3\ {\rm km\,s^{-1}}$, $K = (5.9\pm0.1)\times10^4\ {\rm km\,s^{-1}}$, and $\xi\sim145^\circ$, and $K_S = -4.254$. Here we set B_H and B_K to zero, which is consistent with the error estimates in [27]

Additional corrections from the *hangup kick* effect, and a new effect, which we will dub the *cross kick* effect, are examined here. We note that these new effects were found using equal-mass BHBs, thus their dependence on mass ratio is still speculative.

In our recent studies of BHB mergers we found that nonlinear terms in the spin play an important role in modeling recoil velocities [21]. Here we will investigate higher-order models for the recoil velocity based on the symmetry properties of its components [32]. In Boyle *et al* [32] a new method for developing empirical formulas for the remnant BH properties was proposed. This new method was based on a Taylor expansion and using symmetry properties to limit the total number of terms. We combine the two methods by using PN-inspired variables for a Boyle *et al* type of expansion. Fundamental to this construction is the behavior of the BHB under discrete operations such as exchange (X) of the black holes labels $(1 \longleftrightarrow 2)$ and parity (P) $(x\to-x, y\to-y, z\to-z)$.

A. Comparing Expansion Variables

We model higher-order contributions to the recoil using the PN variables $\vec{\Delta}$, $\vec{S}$, η, and δm [26]. Note that we could use an alternative set of variables, which at first glance would appear to be simpler, such as $\vec{S}^{\pm}/m^2 = (\vec{S}_1 \pm \vec{S}_2)/m^2$ and dropping an explicit η dependence (which can be reabsorbed in δm). For example, in recoil contribution due to unequal mass can be expressed as

$$V_m = a.\delta m + b.\delta m^3 + \cdots, \tag{3}$$

and because

$$\eta = (1 - \delta m^2)/4, \tag{4}$$

this is equivalent to the more usual (See Eq. (2) above)

$$V_m = \eta^2.\delta m.(A + B.\eta + \cdots) \tag{5}$$

The same equivalence can be shown for the variable $\vec{\Delta} = m.(\vec{S}_2/m_2 - \vec{S}_1/m_1)$. That is, since

$$q = (1 - \delta m)/(1 + \delta m), \tag{6}$$

we find

$$\vec{\Delta} = (\vec{S}_2 - \vec{S}_1) - 2.\delta m.(\vec{S}_2 + \vec{S}_1) + 2.\delta m^2.(\vec{S}_2 - \vec{S}_1) + \ldots, \tag{7}$$

and hence $\vec{\Delta}$ can be reexpressed in terms of the alternative spin variables.

We can investigate which choices of expansion variables give the best fits with the fewest number of terms. For example, we can explore if the variables $\vec{S}$ and $\vec{\Delta}$ are really more advantageous then the pair $\vec{S}_{\pm}$. To verify that the leading-order contribution to the out-of-plane recoil is best fit using $\vec{\Delta}$, we revisit the results from a previous paper [28], where we considered the case of a larger spinning BH, with spin in the orbital plane, and a smaller nonspinning BH. In Fig. 2, we show the results of fitting those data to the forms

$$V_{\|} \approx \frac{K 2^{b-1} \alpha_2 \eta^2}{(1+q)^b}, \text{ and } V_{\|} \approx \frac{K \alpha_2 (4\eta)^{b'}}{16(1+q)^2}.$$

The former assumes a leading η^2 dependence, but distinguishes between $\Delta_\perp$ (i.e. $\alpha_2/(1+q)$) and $S_\perp^-$ (i.e. $\alpha_2/(1+q)^2$), while the latter is used to find the best leading power of η assuming the spin-dependence is proportional to S^- and by choosing functions that reproduce the equal-mass limit. We find that the best fit parameters are, $b = 0.993 \pm 0.038$, and, $b' = 3.3 \pm 0.2$. The results clearly indicate that the leading-order recoil is best fit by $\eta^2 \Delta_\perp$.

After finding that the *superkick* effect is best modeled using $\eta^2 \vec{\Delta}$ as the spin variable, we can motivate our ansatz for a leading η^2 for the remaining spin-dependent terms in our empirical formula without appealing to PN theory. To do this, we examine the particle limit and use perturbation theory. Perturbative theory applies in the small-mass-ratio limit, but is otherwise a relativistic theory, and unlike the post-Newtonian approximations, it applies in the strong, highly-dynamical, regime.

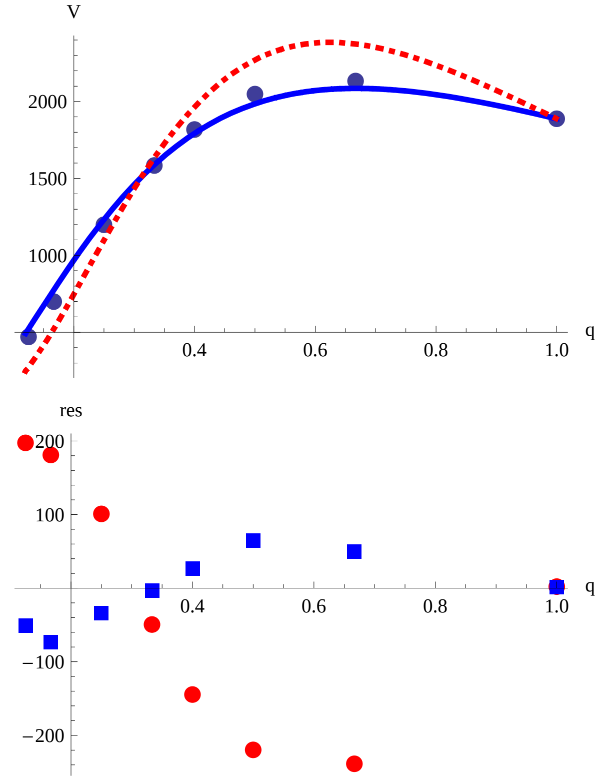

FIG. 2: A fit of the data from [28] to determine if the leading dependence of the recoil is proportional to $\Delta_\perp$ (blue) or S^- (red - dotted). The fits were constructed to reproduce the same equal-mass limit.

Since the radiative perturbative modes are proportional to q, and the radiation of the linear momentum is proportional to surface integrals of squares of these modes, the instantaneous radiated linear momentum is proportional to q^2 (which, by symmetry considerations, generalizes to η^2).

For the linear-in-spin terms, one can use the decomposition in Ref. [33], where the spin of the large black hole is considered a perturbation of a nonrotating, Schwarzschild BH. Since this is a dipolar (Odd) $\ell = 1$ term, it is nonradiative, and, in order to generate a radiative term, it must be coupled with an $\ell \geq 2$ radiative perturbation. To generate linear momentum, this spin-dependent radiative mode must couple with a non-spin dependent radiative mode (otherwise the spin would enter at quadratic order). Again, the leading-order terms in the recoil are proportional to q^2.

TABLE I: Symmetry properties of key quantities

Symmetry	P	X
$S_\perp/m^2 = (S_1+S_2)_\perp/m^2$	−	−
$S_\parallel/m^2 = (S_1+S_2)_\parallel/m^2$	+	+
$\Delta_\perp/m^2 = (S_2/m_2 - S_1/m_1)_\perp/m$	+	−
$\Delta_\parallel/m^2 = (S_2/m_2 - S_1/m_1)_\parallel/m$	−	+
$\hat{n} = \hat{r}_1 - \hat{r}_2$	+	−
$\delta m = (m_1 - m_2)/m$	+	−
$V_\perp$	+	−
$V_\parallel$	−	+

TABLE II: Number of possible terms at a given order of expansion (with respect to $\vec{S}$ or $\vec{\Delta}$). Here 1 indicates terms present even in the equal-mass limit (and/or proportional to even powers of δm) and δm indicates terms proportional to δm to odd powers.

Order	0th	0th	1st	1st	2nd	2nd	3rd	3rd	4th	4th	total
mass	1	δm	1	δm	1	δm	1	δm	1	δm	All
$V_\parallel$	0	0	1	1	2	2	5	5	8	8	32
$V_\perp$	0	1	1	1	2	4	5	5	8	11	38
Total	0	1	2	2	4	6	10	10	16	19	70

B. Symmetry considerations

A Taylor expansion of a function with v independent variables of a given order of expansion o has n terms, where n is given by [34]

$$n = \frac{(o+v-1)!}{o!\,(v-1)!}. \tag{8}$$

However, only certain combinations of variables are allowed. In order to take into account the correct combinations of variables for each component of the recoil velocity at a given order, we consider the symmetry properties summarized in Table I. The possible terms to a given expansion order in spin (i.e., products of S and Δ) are summarized in Tables II-IV. The terms in Tables III and IV are all multiplied by fitting coefficients. Note that the coefficients of these terms can depend on higher powers of δm (even powers for terms proportional to δm^0 and odd powers for terms proportional to δm).

TABLE III: Parameter dependence at each order of expansion for the off-plane recoil. Here 1 indicates terms present even in the equal-mass limit (and/or proportional to even powers of δm) and δm indicates terms proportional to δm to odd powers.

$V_\parallel$	0th order
1	0
δm	0
$V_\parallel$	1st order
1	$\Delta_\perp$
δm	$S_\perp$
$V_\parallel$	2nd order
1	$\Delta_\perp.S_\parallel + \Delta_\parallel.S_\perp$
δm	$\Delta_\perp.\Delta_\parallel + S_\perp.S_\parallel$
$V_\parallel$	3rd order
1	$\Delta_\parallel.S_\perp.S_\parallel + \Delta_\perp.S_\parallel^2 + \Delta_\perp.\Delta_\parallel^2 + \Delta_\perp^3 + \Delta_\perp.S_\perp^2$
δm	$S_\perp.\Delta_\parallel^2 + S_\perp.S_\parallel^2 + \Delta_\perp.\Delta_\parallel.S_\parallel + S_\perp.\Delta_\perp^2 + S_\perp^3$
$V_\parallel$	4th order
1	$S_\perp.\Delta_\parallel^3 + \Delta_\perp.S_\parallel^3 + \Delta_\perp.S_\parallel.\Delta_\parallel^2 + S_\perp.\Delta_\parallel.S_\parallel^2 + \Delta_\perp^3.S_\parallel + S_\perp^3.\Delta_\parallel + \Delta_\perp^2.S_\perp.\Delta_\parallel + \Delta_\perp.S_\perp^2.S_\parallel$
δm	$\Delta_\perp.\Delta_\parallel^3 + S_\perp.S_\parallel^3 + S_\perp.S_\parallel.\Delta_\parallel^2 + \Delta_\perp.\Delta_\parallel.S_\parallel^2 + \Delta_\perp^3.\Delta_\parallel + S_\perp^3.S_\parallel + \Delta_\perp^2.S_\perp.S_\parallel + S_\perp^2.\Delta_\perp.\Delta_\parallel$

Interestingly, for the $\delta m-$independent terms, we can obtain the spin-dependence of the in-plane recoil from the spin-dependence of the out-of-plane recoil via

$$V_\perp = V_\parallel[\Delta_\perp \longleftrightarrow \Delta_\parallel], \tag{9}$$

while for the $\delta m-$dependent terms that are odd powers in the spin variables, we have

$$V_\perp(\delta m) = \delta m.V_\parallel[S_\perp \longleftrightarrow S_\parallel]. \tag{10}$$

On the other hand, for terms proportional to even powers of the spin variables there are extra terms not present in $V_\parallel$.

In addition, functionally, the terms proportional to δm in $V_\parallel$ can be obtained from the δm-independent terms in $V_\parallel$ by

$$V_\parallel(\delta m) = \delta m.V_\parallel[S_\perp \longleftrightarrow \Delta_\perp], \tag{11}$$

while for odd powers of the spins *only*, the δm-dependent terms in $V_\perp$ can be obtained from the δm-independent terms via

$$V_\perp(\delta m) = \delta m.V_\perp[S_\parallel \longleftrightarrow \Delta_\parallel]. \tag{12}$$

TABLE IV: Parameter dependence at each order of expansion for the in-plane recoil. Here 1 indicates terms present even in the equal-mass limit (and/or proportional to even powers of δm) and δm indicates terms proportional to δm to odd powers.

$V_\perp$	0th order
1	0
δm	1
$V_\perp$	1st order
1	$\Delta_\parallel$
δm	$S_\parallel$
$V_\perp$	2nd order
1	$\Delta_\parallel.S_\parallel + \Delta_\perp.S_\perp$
δm	$\Delta_\parallel^2 + S_\parallel^2 + \Delta_\perp^2 + S_\perp^2$
$V_\perp$	3rd order
1	$\Delta_\perp.S_\perp.S_\parallel + \Delta_\parallel.S_\parallel^2 + \Delta_\parallel.\Delta_\perp^2 + \Delta_\parallel^3 + \Delta_\parallel.S_\perp^2 + \Delta_\parallel^3$
δm	$S_\parallel.\Delta_\parallel^2 + S_\parallel.S_\perp^2 + \Delta_\perp.S_\perp.\Delta_\parallel + S_\parallel.\Delta_\perp^2 + S_\parallel^3$
$V_\perp$	4th order
1	$S_\perp.\Delta_\perp^3 + \Delta_\parallel.S_\parallel^3 + \Delta_\parallel.S_\parallel.\Delta_\perp^2 + S_\perp.\Delta_\perp.S_\parallel^2 + \Delta_\parallel^3.S_\parallel + S_\perp^3.\Delta_\perp + \Delta_\parallel^2.S_\perp.\Delta_\perp + \Delta_\parallel.S_\perp^2.S_\parallel$
δm	$\Delta_\perp.\Delta_\parallel.S_\perp.S_\parallel + \Delta_\perp^4 + \Delta_\parallel^4 + S_\perp^4 + S_\parallel^4 + \Delta_\perp^2.\Delta_\parallel^2 + \Delta_\perp^2.S_\perp^2 + \Delta_\perp^2.S_\parallel^2 + \Delta_\parallel^2.S_\perp^2 + \Delta_\parallel^2.S_\parallel^2 + S_\perp^2.S_\parallel^2$

No such correspondence holds for the for the δm-dependent terms with odd powers in the spin for $V_\perp$.

C. The equal-mass case

Using the above properties we find 16 terms up to fourth-order in the spin that contribute to the off-plane recoil velocity

$$\begin{aligned} V_\parallel = \; & \Delta_\perp + \Delta_\perp.S_\parallel + \Delta_\parallel.S_\perp + \\ & \Delta_\perp.\Delta_\parallel^2 + \Delta_\perp^3 + \Delta_\perp.S_\parallel^2 + \\ & \Delta_\perp.S_\perp^2 + \Delta_\parallel.S_\perp.S_\parallel + \\ & \Delta_\perp^3.S_\parallel + \Delta_\parallel.S_\perp^3 + \Delta_\parallel^3.S_\perp + \Delta_\perp.S_\parallel^3 + \\ & \Delta_\parallel.S_\perp.S_\parallel^2 + \Delta_\parallel.\Delta_\perp^2.S_\perp + \\ & \Delta_\perp.S_\parallel.\Delta_\parallel^2 + \Delta_\perp.S_\parallel.S_\perp^2 + \cdots \end{aligned} \quad (13)$$

We can regroup all these terms (assuming we can collect all $\perp$ terms) in the following form

$$\begin{aligned} V_\parallel = \; & \Delta_\perp.(1 + \Delta_\perp^2 + \cdots).(1 + \Delta_\parallel^2 + \cdots). \\ & .(1 + S_\perp^2 + \cdots).(1 + S_\parallel + S_\parallel^2 + S_\parallel^3 + \cdots) + \\ & + S_\perp.\Delta_\parallel.(1 + \Delta_\perp^2 + \cdots).(1 + \Delta_\parallel^2 + \cdots). \\ & .(1 + S_\perp^2 + \cdots).(1 + S_\parallel + S_\parallel^2 + \cdots). \end{aligned} \quad (14)$$

The 10 terms directly proportional to the $\cos(\varphi)$ are those linear to the subindex $\perp$

$$\begin{aligned} V_\parallel^{\cos\varphi} = \; & \Delta_\perp.(1 + \Delta_\parallel^2 + \cdots).(1 + S_\parallel + S_\parallel^2 + S_\parallel^3 + \cdots) + \\ + \; & S_\perp.\Delta_\parallel.(1 + \Delta_\parallel^2 + \cdots).(1 + S_\parallel + S_\parallel^2 + \cdots) \end{aligned} \quad (15)$$

This (symbolic) expression is the one we will use in this paper.

There is a subtlety in the above expansion. Because $S_\perp$ and $\Delta_\perp$ are vector quantities, terms like $\Delta_\perp(1+S_z+\cdots)$, etc., should really be expressed as $C_1\vec{\Delta}\cdot\hat{n}_1 + C_2\vec{\Delta}\cdot\hat{n}_2 S_z + \cdots$, where $\hat{n}_1$ and $\hat{n}_2$ are unit vectors in the plane, i.e., not only are there fitting constants $C_1, C_2, \cdots$, but each coefficient also has its own angular dependence. We will return to this issue in Sec. VI.

III. NUMERICAL RELATIVITY TECHNIQUES

For the black-hole binary (BHB) data presented here, both BHs have the same mass, but have different spins. We use the TwoPunctures thorn [35] to generate initial puncture data [36] for the BHB simulations described below. These data are characterized by mass parameters $m_{p1/2}$, momenta $\vec{p}_{1/2}$, spins $\vec{S}_{1/2}$, and coordinate locations $\vec{x}_{1/2}$ of each hole. We obtain parameters for the location, momentum, and spin of each BH using the 2.5 PN quasicircular parameters. Here we choose to normalize the PN initial data such that the total Arnowitt-Deser-Misner (ADM) energy is $1M$. We obtain parameters $m_{p1/2}$ using an iterative procedure in order to obtain a system where the two BHs have the same mass and the total ADM energy is $1M$. This iterative procedure is most efficient when the horizon masses and ADM energy can be obtained from the initial data alone. For highly-spinning BHs ($\alpha = S/m^2 \gtrsim 0.9$), a relatively large amount of energy lies outside the BH. This energy is eventually absorbed, changing the mass of the BH substantially (see, e.g. [37]). We therefore limit the spin of the BHs to $\alpha =\leq 0.8$ for all but a few simulations.

We evolve these BHB data sets using the LazEv [38] implementation of the moving puncture approach [2, 3] with the conformal function $W = \sqrt{\chi} = \exp(-2\phi)$ suggested by Ref. [39]. For the runs presented here, we use centered, eighth-order finite differencing in space [40] and a fourth-order Runge Kutta time integrator. (Note that we do not upwind the advection terms.)

Our code uses the EinsteinToolkit [41, 42] / Cactus [43] / Carpet [44] infrastructure. The Carpet mesh refinement driver to provide a "moving boxes" style of mesh refinement. In this approach refined grids of fixed size are arranged about the coordinate centers of both holes. The Carpet code then moves these fine grids about the computational domain by following the trajectories of the two BHs.

We obtain accurate, convergent waveforms and horizon parameters by evolving this system in conjunction with a modified 1+log lapse and a modified Gamma-driver shift condition [2, 45, 46], and an initial lapse $\alpha(t=0) = 2/(1+\psi_{BL}^4)$, where ψ_{BL} is the Brill-Lindquist conformal factor and is given by

$$\psi_{BL} = 1 + \sum_{i=1}^{n} m_i^p/(2|\vec{r} - \vec{r}_i|),$$

where $\vec{r}_i$ is the coordinate location of puncture i. The lapse and shift are evolved with

$$(\partial_t - \beta^i\partial_i)\alpha = -2\alpha K, \quad (16a)$$

$$\partial_t\beta^a = (3/4)\tilde{\Gamma}^a - \eta\beta^a\,, \quad (16b)$$

where we use $\eta = 2$ for all simulations presented below.

We use AHFinderDirect [47] to locate apparent horizons. We measure the magnitude of the horizon spin using the *isolated horizon* (IH) algorithm detailed in Ref. [48]. Note that once we have the horizon spin, we can calculate the horizon mass via the Christodoulou formula

$$m_H = \sqrt{m_{\rm irr}^2 + S_H^2/(4m_{\rm irr}^2)}\,, \quad (17)$$

where $m_{\rm irr} = \sqrt{A/(16\pi)}$ and A is the surface area of the horizon, and S_H is the spin angular momentum of the BH (in units of M^2). In the tables below, we use the variation in the measured horizon irreducible mass and spin during the simulation as a measure of the error in these quantities. We measure radiated energy, linear momentum, and angular momentum, in terms of the radiative Weyl Scalar ψ_4, using the formulas provided in Refs. [49, 50]. However, rather than using the full ψ_4, we decompose it into ℓ and m modes and solve for the radiated linear momentum, dropping terms with $\ell \geq 5$. The formulas in Refs. [49, 50] are valid at $r=\infty$. We extract the radiated energy-momentum at finite radius and extrapolate to $r=\infty$ using both linear and quadratic extrapolations. We use the difference of these two extrapolations as a measure of the error.

Both the remnant parameter variation, and the variation in the extrapolation to infinity of the radiation underestimate the actual errors in the quantity of interest. However, because quantities like the total radiated energy can be obtained from either extrapolations of ψ_4 or, quite independently, from the remnant BHs mass, the difference between these two is a reasonable estimate for the actual error.

Our empirical formula will depend on the spins measured with respect to the orbital plane at merger. In Ref [28] we described a procedure for determining an approximate plane. This is based on locating three fiducial points on the BHBs trajectory $\vec{r}_+$, $\vec{r}_0$, and $\vec{r}_-$, where $\vec{r}_+$ is the point where $\ddot{r}(t)$ ($r(t)$ is the orbital separation) reaches its maximum, $\vec{r}_-$ is the point where $\ddot{r}(t)$ reaches its minimum, and $\vec{r}_0$ is the point between the two where $\ddot{r}(t) = 0$. These three points can then be used to define an approximate merger plane (see Fig. 3). We then need to rotate each trajectory such that the infall directions all align (as much as possible). This is accomplished by rotating the system, keeping the merger plane's orientation fixed, such that the vector $\vec{r}_+ - \vec{r}_0$ is aligned with the y axis. The azimuthal angle φ, described below, is measured in this rotated frame.

Our motivation for defining the orbital plane "at merger" is the observation that most of the recoil is generated near (and slightly after) merger. For example, Fig. 4 shows the recoil imparted to the remnant BH for the N45PH30 configuration. As seen in the plot, all but 16% of the recoil is generated "post-merger."

IV. SIMULATIONS

In this paper we consider four families of equal-mass, precessing, BHB configurations, which we will denote by S, K, L, and N. Initial data parameters are given in Tables XI and XII (found in Appendix A 1). These configurations are characterized by the spins of the two BHs on the initial slice. For 83 of the 88 simulations, the intrinsic spin of each BH in the binary $\alpha_i = 0.8$, with the exception of the N configurations, where the first BH has spin $\alpha_1 = 0.8$ and the second is nonspinning. We also evolved a set of five N configuration (denoted by N9 below) where the spin of BH1 is $\alpha_1 = 0.9$.

For the S configurations, $\vec{S}_1 = -\vec{S}_2$, i.e., the total spin $\vec{S}$ is initially zero, while for the K configurations $S_{1z} = -S_{2z}$ but $S_{1x} = S_{2x}$ and $S_{1y} = S_{2y}$. The L configurations have the spin of BH1 entirely in the orbital plane, while the spin of BH2 is perpendicular to the plane, and finally the N configurations have BH1 spinning and BH2 nonspinning. We use the notation zTHxxxPHyyy, where z is N, N9, S, K, or L, xxx gives the inclination angle θ of spin of BH1 and yyy gives the orientation of the spin of BH1 in the initial orbital plane, i.e. the azimuthal angle ϕ. In order to fit the resulting recoils, we found that we needed at least six azimuthal configurations in the interval $[0, 180^\circ)$ for each θ configurations. This is due to the fact that we need to separate contributions due to $\cos 3\phi$ from contributions due to $\cos\phi$ (by symmetry, the recoil out of the plane cannot contain terms of the form $\cos n\phi$ if n is even).

In all cases but N9, the computational domain extended to $\pm 400M$, with a coarsest resolution of $h = 4M$

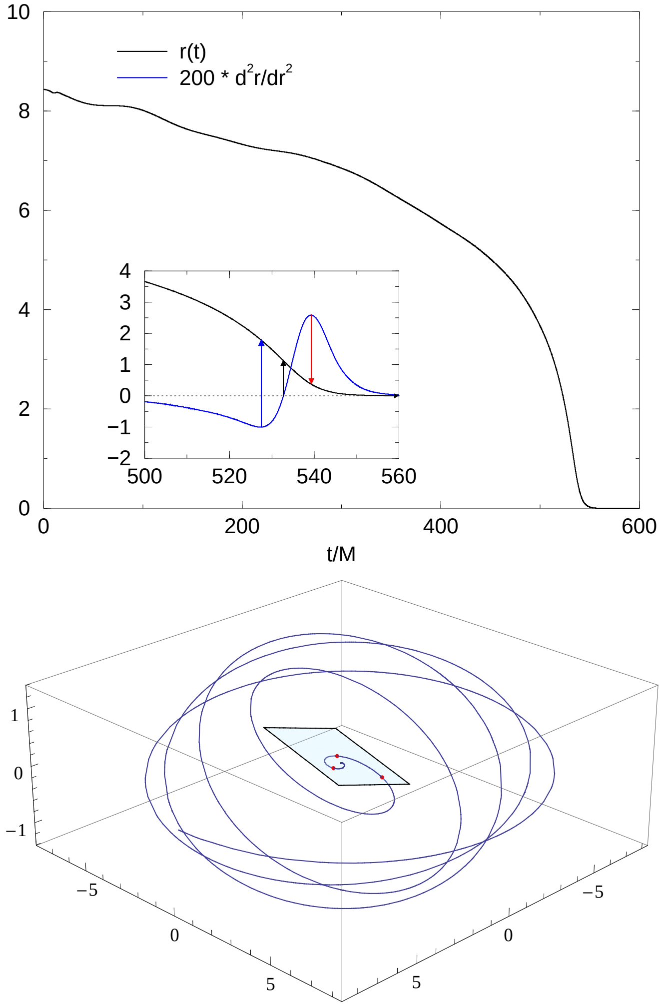

FIG. 3: Finding the orbital plane near merger. The upper plot shows the orbital separation $r(t)$ versus time. The inset shows $r(t)$ near merger and $\ddot{r}(t)$ (rescaled by 200 for clarity). The points $\vec{r}_+$, $\vec{r}_0$, and $\vec{r}_-$ correspond to the times where $\ddot{r}$ is maximized, zero, and minimized (denoted with arrows here). The plot below shows the trajectory, the points $\vec{r}_+, \vec{r}_0, \vec{r}_-$ (large red dots) and the "merger" plane.

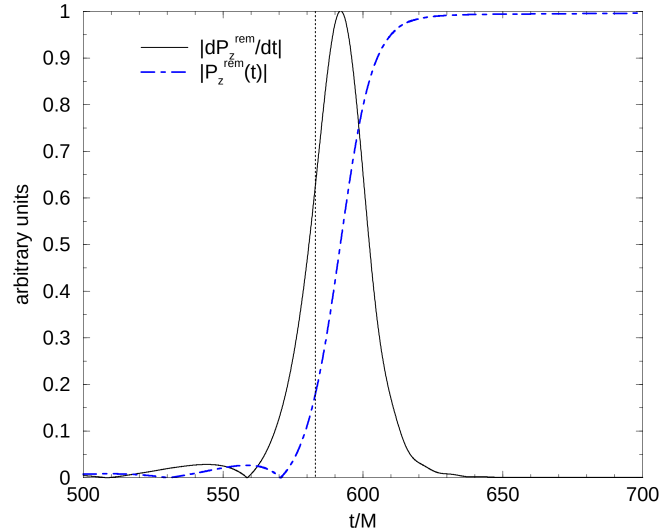

FIG. 4: A plot of the absolute values of $P_z(t)$ (the momentum imparted to the remnant) and $dP_z/dt(t)$ for NTH45PH30 configuration. The vertical line represents the approximate time of merger.

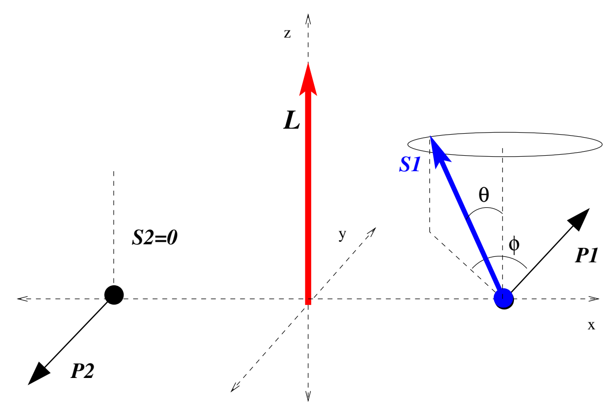

FIG. 5: The N configuration. These configurations differ from the *hangup kick* configurations in that BH2 is nonspinning. Numerical evolutions preserve the N configurations only approximately.

at the outer boundary. We used 9 levels of refinement, centered on each puncture, with radii 200, 100, 50, 20, 10, 5, 2, 0.6, respectively. For the N9 configurations, the computational domain extended to $\pm 400M$, with a coarsest resolution of $h = 3.33M$, and we used an additional level of refinement about BH1, with radius 0.35.

We chose these configurations for two main reasons, first each family of configurations can be described by a single azimuthal angle parameter ϕ and a single polar angle θ, and they activate different terms in our ansatz for the recoil. The former is necessary in order to reduce the computational costs. In general, four angular parameters are required in order to describe the spins at merger (two polar and two azimuthal). In order to model the polar and azimuthal dependence, we would need at least $6\times6\times6\times6 = 1296$ simulations (per choice of spin magnitude, per choice of mass ratio). By reducing the dimensionality to two, we only need 36 simulations (per family, per α, per q). This reduction only works, however, if the two parameter family of initial data, maps in a straightforward way to a 2 parameter family of configurations at merger. In particular, we need the final configuration to be describable by a single azimuthal and polar angle. We note that this is not the case in general, and that we used PN simulations to tests the stability of various configurations. For the N configuration, the mapping to a single azimuthal angle is automatic because only one BH is spinning, for the other configurations, we verify that the configuration can be described by a single angle by comparing four different measurements of the azimuthal angle. The results are displayed in Table V, which shows

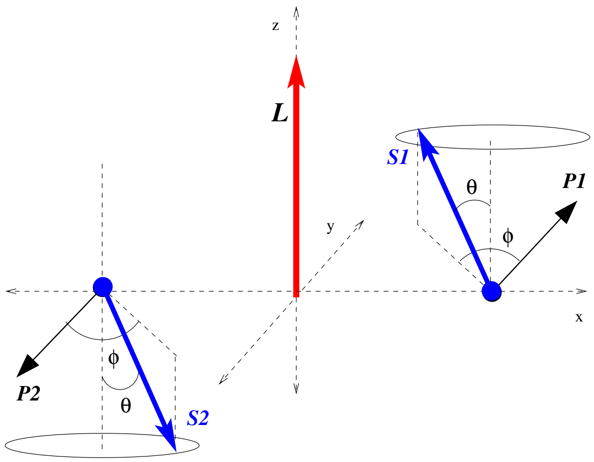

FIG. 6: The S configuration. These configuration differ from the *hangup kick* configuration in that $S_{1z} = -S_{2z}$ (and hence $\vec{S}_1 = -\vec{S}_2$), initially. Numerical evolutions preserve the S configurations only approximately.

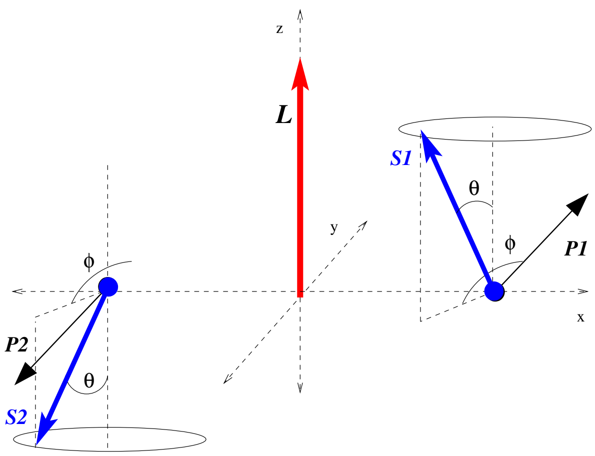

FIG. 7: The K configuration. These can be thought of as a modification of the S configurations. There $S_{1z} = -S_{2z}$, while $S_{1x} = S_{2x}$ and $S_{1y} = S_{2y}$, initially.

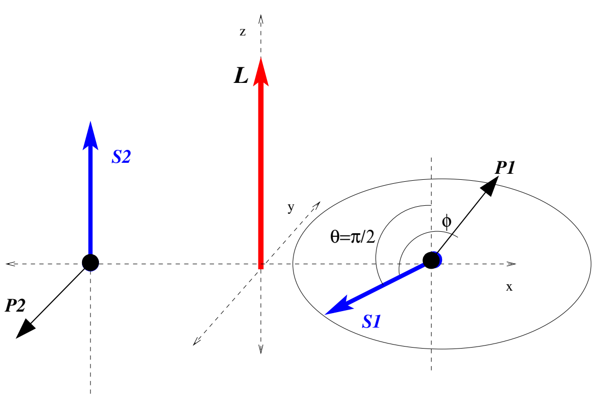

FIG. 8: The L configuration. The L configuration is a modification of the N configuration, where S_1 is aligned with the orbital angular momentum $\hat{z}$ and rather than having $S_2 = 0$, $\vec{S}_2$ is varied initially in the orbital plane.

TABLE V: S, K, and L configuration angles. Here ϕ_1 is the angle between the in-plane component of $\vec{S}_1$ for configuration PH0 and the corresponding PHXX configuration, while ϕ_2 is defined using $\vec{S}_2$, ϕ_Δ using $\vec{\Delta}$, and ϕ_S using $\vec{S}$. These angles agree to within $(3-15)^\circ$, which justifies our using a single angle in our fitting formula for this configuration. For the S configurations, ϕ_S is ill-defined since $S_\perp$ is very small.

Conf	ϕ_1	ϕ_2	ϕ_Δ	ϕ_S
STH45PH0	0	0	0	0
STH45PH30	33.3518	30.9202	32.0924	
STH45PH60	61.7152	58.2499	59.9753	
STH45PH90	91.4444	88.5921	90.0456	
STH45PH120	116.271	115.641	115.997	
STH45PH90	143.981	144.881	144.46	
KTH45PH0	0	0	0	0
KTH45PH30	28.6011	31.0559	31.4676	28.8129
KTH45PH60	39.3732	41.6249	42.4836	39.2248
KTH45PH90	58.7044	59.2109	61.8581	56.8317
KTH45PH105	75.1457	72.9151	76.7906	71.6609
KTH45PH120	95.7513	90.7761	95.0918	91.3502
KTH45PH135	114.209	108.253	112.123	110.072
KTH45PH150	135.705	130.366	133.203	132.59
KTH45PH165	156.52	153.385	154.838	154.882
KTH22.5PH0	0	0	0	0
KTH22.5PH30	29.9	23.9	26.8	25.12
KTH22.5PH60	52.1	42.1	45.7	46.3
KTH22.5PH90	71.4	59.8	62.8	71.4
KTH22.5PH120	101.2	92.8	92.9	102.2
KTH22.5PH150	142.5	143.4	139.9	147.5
LPH0	0	0	0	0
LPH30	17.9	20.8	17.0	24.7
LPH60	35.0	36.3	32.0	45.3
LPH90	55.2	52.3	49.8	65.3
LPH120	87.6	80.0	81.4	93.0
LPH150	139.9	130.8	136.1	138.4

that, to within about 3-15 degrees, the configurations are describable by a single angle.

V. RESULTS

Results from these 88 simulations are given in the tables in Appendix A 2 below. In Tables XIII and XIV we give the remnant BH mass and spin, as measured using the IH formalism, while in Tables XV and XVI, we give the radiated energy, angular momentum, and recoil, as calculated from the waveform extracted at $60M, 70M, \cdots, 100M$ and then extrapolated to infinity. We compare these two independent measures in Tables XVII and XVIII. Finally, in Tables XIX and XX, we give the spin of each BH near merger, and the final remnant recoil, in a rotated frame aligned with averaged orbital angular momentum at merger. For completeness, we also show in Table XXI the value of $\Delta_\perp$, $S_\perp$, Δ_z, and S_z corresponding to the BH spin in Table XIX.

In order to analyze the results of the present simulations, we use the techniques developed in [28]. Briefly, we rotate each configuration such that the trajectories near merger overlap. We then calculate the spins in this rotated frame. This is done separately for each family of constant θ per configuration type (S,L,K,N). The angle φ is then defined to be the angle (at merger) between spin of BH1 (the BH originally located on the positive x axis) for a given PHyyy configuration and the spin of BH1 in the corresponding PH0 configuration. Note that, for a given family of fixed spin and spin inclination angle θ, the angle φ and ϕ differ by a constant, which can be absorbed in the fitting constants ϕ_1 and ϕ_3. We then fit the recoil in these sub-families to the form

$$V_{\rm rec} = V_1 \cos(\varphi - \phi_1) + V_3 \cos(3\varphi - 3\phi_3). \tag{18}$$

Our tests indicate that V_1 can be obtained accurately with 6 choices of the initial ϕ_i angles. For example, a fit all the NTH45PHyyy gives $V_1 = 1349.0 \pm 9.7$ if we include all 12 angles (see Table XIX), and $V_1 = 1346 \pm 22$ if we include 6 angles.

In all cases, V_3 is much smaller than V_1. Results from these fits are given in Table VI and Fig. 9. We note that there are additional approximations inherent in this procedure. To demonstrate this, consider the formula

$$V_z = \Delta_\perp (A + B S_z + \cdots) + S_\perp \Delta_z (D + E S_z + \cdots), \tag{19}$$

where A, B, C, D, E are fitting constants. Even when considering "symmetric" configurations like S, K, L, and N, where $\vec{S}$ and $\vec{\Delta}$ cannot rotate independently, each term in Eq. (19) may be maximized at different azimuthal angles, and the formula should really be written as

$$\begin{aligned} V_z = & A \vec{\Delta} \cdot \hat{n}_0 + B \vec{\Delta} \cdot \hat{n}_1 S_z + \cdots \\ & + D \vec{S} \cdot \hat{n}_2 \Delta_z + E \vec{S} \cdot \hat{n}_3 \Delta_z S_z + \cdots , \end{aligned} \tag{20}$$

where $\hat{n}_i$ are unit vectors in the orbital plane. If we make the additional assumption that the coefficient A dominates this expression, then Eq. (20) can be approximated by

$$\begin{aligned} V_z = & \vec{\Delta} \cdot \hat{n}_0 (A + B \cos(\vartheta_1) S_z) \\ & + \vec{S}_\perp \cdot \hat{n}_0 \Delta_z (D \cos(\vartheta_2) + E \cos(\vartheta_3) S_z), \end{aligned} \tag{21}$$

where ϑ_i is the angle between $\hat{n}_i$ and $\hat{n}_0$. There will be terms proportional to $\sin \vartheta_i$, but they will be $\mathcal{O}(1/A)$, which we will assume to be small enough to ignore. If, in addition, we assume that the angles ϑ_i do not vary significantly between different configurations, then we can replace the fitting constants in Eq. (21) by the product of the constant with the corresponding $\cos \vartheta_i$. We can then interpret V_1 from Eq. (18) as the $V_1 = |\Delta_\perp|(A + \tilde{B} S_z) + |S_\perp||\Delta_Z|(\tilde{D} + \tilde{E} S_z)$, where $\tilde{B} = B \cos \vartheta_1$, etc. Ultimately, we justify all our approximations by testing the resulting formula using several different families of configurations.

The N configurations are the only ones with families of different θ (apart from the two angles for the K configuration). For these families, we fit the data in Table VI

TABLE VI: A fit of the recoil for each family of PHYYY configurations to the form $V_\parallel = V_1 \cos(\varphi - \phi_1) + V_3 \cos(3\varphi - 3\phi_3)$. Note how the K configurations, which started with $\Delta_\perp = 0$, evolved to configurations with large $\Delta_\perp$.

CONF	V_1	V_3	ϕ_1	ϕ_3
NTH15	539.34 ± 2.5	33.2 ± 2.3	141.96 ± 0.24	297.1 ± 1.3
NTH30	1002 ± 12	43 ± 13	126.42 ± 0.71	260.3 ± 5.3
NTH45	1349.0 ± 9.7	52 ± 12	82.50 ± 0.58	337.0 ± 3.9
NTH60	1542 ± 11	34 ± 11	20.83 ± 0.47	269.2 ± 6.8
NTH120	1199 ± 13	37 ± 12	292.79 ± 0.54	139.6 ± 5.9
NTH135	927.5 ± 6.4	35.6 ± 6.7	226.90 ± 0.43	311.3 ± 3.6
NTH165	312.9 ± 6.4	11.6 ± 6.2	213.4 ± 1.2	189 ± 11
STH45	2020 ± 19	50 ± 19	291.40 ± 0.56	342.3 ± 7.3
KTH45	2227 ± 12	195 ± 12	217.33 ± 0.32	155.0 ± 1.3
KTH22.5	1731 ± 25	130 ± 23	164.49 ± 0.75	100.9 ± 3.4
L	3014 ± 21	145 ± 18	331.30 ± 0.36	263.50 ± 2.9
N9TH55	1803.4 ± 6.2	27.6 ± 6.8	74.89 ± 0.14	102.6 ± 2.8

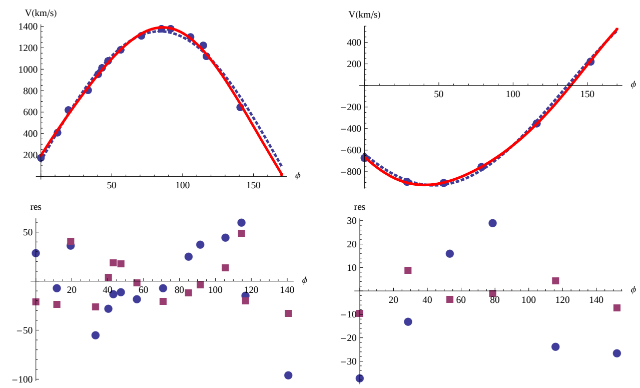

FIG. 9: A fit of the recoil for the NTH45PHyyy (left) and NTH135PHyyy (right) configurations to $V = V_1 \cos(\varphi - \phi_1)$ (blue-dotted) and $V = V_1 \cos(\varphi - \phi_1) + v_3 \cos(3\varphi - 3\phi_3)$ (red-solid), as well as the residuals (blue circles and red squares, respectively). The remaining scatter is due to the fact that $S_\perp$ and S_z vary from configuration to configuration within the NTH45PHyyy and NTH135PHyyy families.

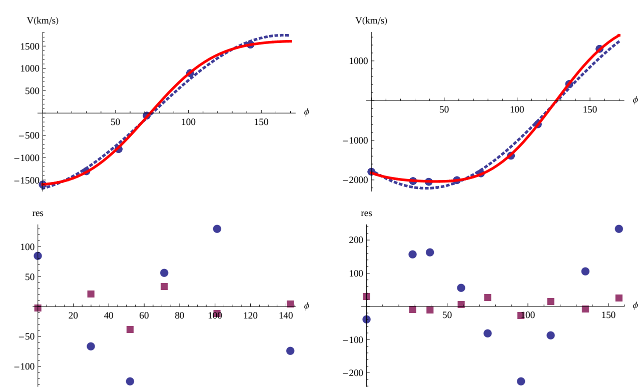

FIG. 10: Fitting of the KTH22.5PHyyy (left) and KTH45PHyyy (right) configurations to $V = V_1 \cos(\varphi - \phi_1)$ (blue-dotted) and $V = V_1 \cos(\varphi - \phi_1) + v_3 \cos(3\varphi - 3\phi_3)$ (red-solid), as well as the residuals (blue circles and red squares, respectively). Note how strong the higher-order contributions are compared to the other configurations.

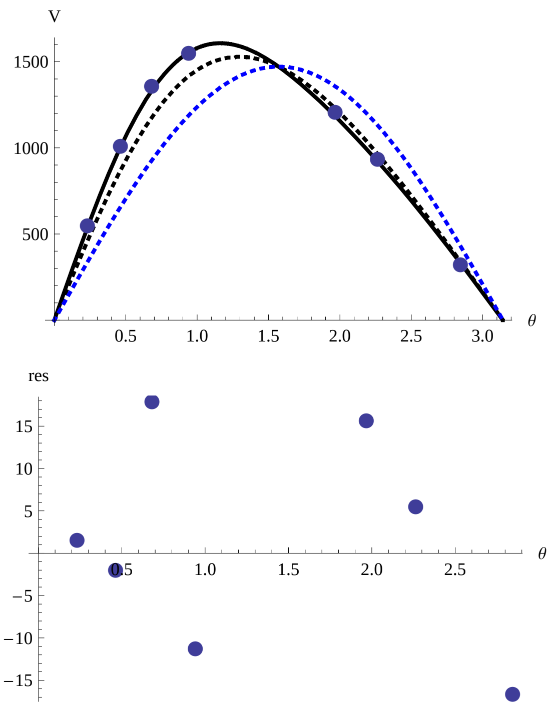

FIG. 11: A fit of the NTHXXX families, with residuals, and comparison with the *hangup kick* formula (black dotted) and *superkick* (more symmetrical, blue-dotted curve). An excess over both formulas at small angles is apparent, while a slight deficit with respect to the *hangup kick* is apparent at large angles.

to the form

$$V_1 = C_1\alpha\sin\theta + C_2\alpha^2\sin\theta\cos\theta + C_3\alpha^3\sin\theta\cos^2\theta + V_{\rm hang}, \quad (22)$$

where $V_{\rm hang}$ is the *hangup kick* [21, 22], which has the form

$$V_{\rm hang} = 3677.76\alpha\sin\theta + 2481.21\alpha^2\sin\theta\cos\theta + 1792.45\alpha^3\sin\theta\cos^2\theta + 1506.52\alpha^4\sin\theta\cos^3\theta. \quad (23)$$

For consistency with our conventions in [21, 22], we define α here to be $\alpha_1/2$. We note that $S_\|/m^2 = (1/2)\alpha$ and $\Delta_\|/m^2 = \alpha$. We also note that, because $\alpha < 1/2$ here, the extrapolation to $\alpha = 1$ is more severe than in the original *hangup kick* configuration. Results from these fits are shown in Table VII. From the table, we can see that the C_1 term is consistent with zero. In subsequent fits, we remove this term and only include C_2 and C_3 (we also attempt a fit including a higher-order C_4 term, but this proved to have an unacceptably large error).

VI. MODELING THE RECOIL VELOCITY

As seen in Sec. II C, when considering the equal-mass case, and spin-contributions up through third-order, the most general formula for the out-of-plane recoil is

$$V_\| = \Delta_\perp(A + BS_\| + CS_\|^2) + S_\perp\Delta_\|(D + ES_\|) + F\Delta_\perp S_\perp^2 + G\Delta_\perp\Delta_\|^2 + H\Delta_\perp^3, \quad (24)$$

where $A - H$ are fitting constants. The first line is part of the *hangup kick* recoil, the second and third are new contributions. The term proportional to G is small (if G were big, then the S configuration recoils would be significantly different from the *hangup kick* prediction). The H term is small, as we saw by evolving *superkick* configuration in [24]. Motivated by the *hangup kick* results, where the series $A + BS_\| + CS_\|^2$ had similarly larger values of A, B, and C, we will assume at this point that the term proportional to E is larger than the term proportional to F.

We therefore interpret the additional terms in Eq. (22) as being proportional to powers of $\Delta_\|$ and $S_\|$ and corrections to the *hangup kick* formula have the form $2C_2S_\perp\Delta_\| + 4C_3S_\perp\Delta_\|S_\|$. Then, if we *assume* the same η^2 mass ratio dependence, our ansatz for the z component of the generic recoil becomes

$$\frac{V_\|}{16\eta^2} = \Delta_\perp\left(3677.76 + 2\times 2481.21S_\| + 4\times 1792.45S_\|^2 + 8\times 1506.52S_\|^3\right) + S_\perp\Delta_\|(2C_2 + 4C_3S_\|). \quad (25)$$

TABLE VII: Fit of the N (see Table VI) to the form $V_1 = C_1\alpha\sin\theta + C_2\alpha^2\sin\theta\cos\theta + C_3\alpha^3\sin\theta\cos^2\theta + C_4\alpha^4\sin\theta\cos^3\theta + V_{\rm hang}$. Also included in parenthesis are the fits we obtain when including N9 results. For the first fit, C_4 was set to zero, for the second C_1 (which was found to be consistent with zero) and C_4 were set to zero. For the third. only C_1 was set to zero. The uncertainty in the C_4 coefficients makes using this term in extrapolative formulas problematic (e.g., the differences in the predicted velocity for N9 is under 1 km s^{-1}). We therefore use the second fit in the analysis below. The values in parenthesis were obtained from fits that used the N9 results.

Coeff.	Correction to *hangup kick*	*hangup kick* term
C_1	-19 ± 21 (-21 ± 31)	3677.76
C_2	1124 ± 128 (1245 ± 177)	2481.21
C_3	2961 ± 679 (3458 ± 962)	1792.45
C_4	0	1506.52
C_1	0	3677.76
C_2	1140 ± 125 (1263 ± 168)	2481.21
C_3	2481 ± 434 (2953 ± 573)	1792.45
C_4	0	1506.52
C_1	0	3677.76
C_2	761 ± 243 (878 ± 392)	2481.21
C_3	2281 ± 393 (2747 ± 596)	1792.45
C_4	4733 ± 2721 (4810 ± 4432)	1506.52

TABLE VIII: Comparison of V_1 as fit from the current data and the predictions of the *superkick*, *hangup kick*, and *cross kick* (new) formulas. Note, there is an ambiguity in the sign of the *cross kick* correction for the S configuration (see text). Cross.(B) refer to the *cross kick* prediction using the second set of coefficients from Table VII (not including the N9 configurations).

CONF	$S_\perp/M^2$	$\Delta_\perp/M^2$	$S_\parallel/M^2$	$\Delta_\parallel/M^2$	V_1	Sup.	Hang.	Cross.(B)
NTH15	0.046 ± 0.004	0.092 ± 0.008	0.196 ± 0.001	-0.392 ± 0.002	539.4 ± 2.3	339.746	463.256	540
NTH30	0.090 ± 0.007	0.179 ± 0.013	0.179 ± 0.003	-0.358 ± 0.007	1002 ± 12	658.497	871.282	1007
NTH45	0.126 ± 0.008	0.252 ± 0.015	0.155 ± 0.006	-0.311 ± 0.013	1349.0 ± 9.7	926.499	1176.76	1329
NTH60	0.161 ± 0.0073	0.323 ± 0.015	0.118 ± 0.010	-0.235 ± 0.020	1542 ± 11	1186.7	1413.2	1548
NTH120	0.184 ± 0.004	0.368 ± 0.008	-0.077 ± 0.010	0.154 ± 0.021	1199 ± 13	1355.8	1279	1185
NTH135	0.154 ± 0.006	0.308 ± 0.011	-0.128 ± 0.007	0.256 ± 0.013	927.5 ± 6.4	1134.46	967.015	927
NTH165	0.059 ± 0.003	0.118 ± 0.007	-0.193 ± 0.002	0.386 ± 0.004	312.9 ± 6.4	434.141	342.312	334
KTH45	0.276 ± 0.002	$0.497 \pm .028$	0.054 ± 0.021	-0.277 ± 0.048	2227 ± 12	1826	1970	2185
KTH22.5	$0.149 \pm .003$	0.400 ± 0.037	0.021 ± 0.008	-0.626 ± 0.025	1731 ± 25	1470	1512	1744
L	0.173 ± 0.016	$0.551 \pm .006$	0.227 ± 0.013	0.103 ± 0.051	3014 ± 21	2026	2928	3009
STH45	0.011 ± 0.004	0.552 ± 0.004	0.005 ± 0.003	-0.5760 ± 0.0015	2020 ± 19	2030.15	2044.94	2059*
N9TH55	0.1642 ± 0.0087	0.323 ± 0.018	0.151 ± 0.010	-0.297 ± 0.019	1803.4 ± 6.2	1208.45	1522.5	1728

We refer to this new contribution to the recoil, which has the form $S_\perp \Delta_\parallel (2C_2 + 4C_3 S_\parallel)$, as the *cross kick* (since $S_\perp \Delta_\parallel$ can be expressed as $\hat{z} \cdot \vec{S} \times (\hat{n} \times \vec{\Delta})$, where $\hat{n}$ is a unit vector in the xy plane). The coefficients C_2 and C_3 were determined using only the N and N9 configurations.

We then verify Eq. (25), *in the equal-mass limit*, by comparing the predictions from the new formula with the maximum recoil obtained from the S, K, and L configurations. Our results are given in Table VIII. The table compares the measured value of V_1 for each family with the predictions of the *superkick*, *hangup kick*, and *cross kick*. In all cases, except S, the *cross kick* provides the most accurate prediction for V_1. The results from the K configurations are particularly interesting since the measured recoils and the *cross kick* predictions are both ~ 200 km s^{-1} larger than the *hangup kick* prediction (a 10-16% effect). For the S configurations, there is an ambiguity in the sign of the *cross kick* kick. This is due to the fact that the *cross kick* correction lies in the same direction as the *hangup kick*. Here, however, $S_\parallel = 0.005 \pm 0.003$ and the small *hangup kick* correction may have the wrong sign. If we assume $S_\parallel$ is really zero or slightly negative, we find that the *cross kick* prediction is the most accurate (with a prediction of 2015 km s^{-1}). On the other hand, the N9 runs appear to show that there are still uncertainties in our modeling.

VII. DISCUSSION

The discovery that the hangup effect contributes significantly to the gravitational recoil of merging black hole binaries [21] implies that nonlinear spin couplings are crucial in describing those recoils. Nonlinear couplings come in a variety of combinations, as described in Sec. II. In order to evaluate which of those terms produce the largest contributions to the total recoil, we performed a large set of new simulations. These 88 simulations of precessing BHBs allowed us to confirm the relevance of the *hangup kick* effect in more generic runs, discover another important term that we named *cross kick* that appears in precessing binaries, and gives more accurate predictions for other families of BHB configurations.

While not as dramatic as the *hangup kick* effect, the *cross kick* may prove to be very important in the non-equal-mass regime. To help elucidate how this new contribution affects the recoil (for a given mass ratio), we plot the maximum recoil for configuration with a given mass ratio and with both BHs maximally spinning. As shown in Fig. 12, the *cross kick* enhances the recoil (up to 600 km s^{-1}) in the moderate mass-ratio range.

To see how the *cross kick* contribution to the recoil affects the net probabilities for large recoils, we revisit the case of the supermassive BH binary with spins aligned via hot and cold accretion [22] and non-aligned BHBs (i.e., dry mergers). Briefly, we consider a set of 10 million binaries chosen randomly with a spin-magnitude distribution and spin inclination angle distribution taken from [22], and a mass ratio distribution taken from [51–53]. We assume a uniform distribution of spin directions in the equatorial plane (see Fig. 13). We find an increased probability of large recoils ($V > 2000$ km s^{-1}) by a factor of ~ 2 (see Table IX). However, to generate these probabilities we used the assumption that all terms in Eq. (25) scale with the mass ratio as $16\eta^2$. This is a strong assumption that we will revisit in an upcoming paper. Additionally, we did not take into account new nonlinear terms proportional to δm that may also prove to be important.

As an aside, we note that the distribution of azimuthal orientations of the spin quantity $\vec{\Delta}_\perp$ near merger may appear to be nonuniform. This is actually most pronounced

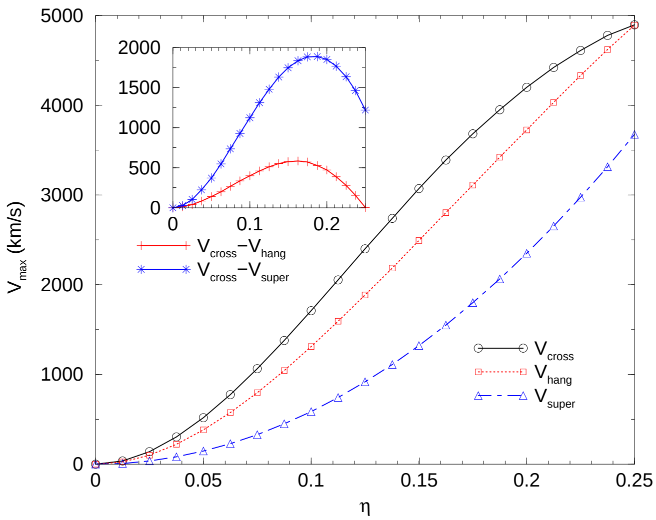

FIG. 12: The maximum recoil velocity predicted by the *cross kick*, *hangup kick*, and *superkick* formulas for BHBs with a given mass ratio and maximal spin. The inset shows the difference between the *cross kick* and *hangup kick* and *cross kick* and *superkick* versus symmetric mass ratio.

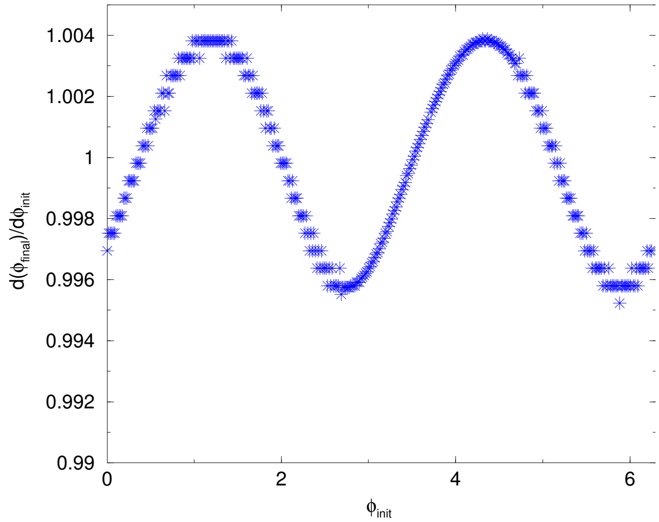

FIG. 13: A plot of $d\phi_{\rm final}/d\phi_{\rm init}$ versus time for a set of 360 binaries in a superkick configuration. The initial separation is $\sim 10M$, while the final separation is $\sim 3M$. The effect is only 4 parts in 1000.

for the $\alpha = 0.9$ in our original *hangup kick* paper [22] (see Fig. 5 there). However, this skew appears to be actually due to varying eccentricity, which leads to different inspiral times for different starting azimuthal configurations. To help confirm that there is not, in fact, a strong preference for any particular azimuthal angles, we evolved as set of 360 superkick configurations (with the spins aligned along $\phi = 0°, 1°, \cdots, 359°$), using 3.5 PN, from a separation of 10M down to 3M (note, we are not concerned with the accuracy of PN at 3M, rather, if there is any significant effect predicted by PN). The distribution of final azimuthal configurations was flat, with no strong preference or clumping. A plot of final versus the initial azimuthal angle ϕ is shown in Fig. 13. There is a small sinusoidal effect at the level of 4 parts in 1000.

On the other hand, the relative orientation of $\vec{S}_{1\perp}$ and $\vec{S}_{2\perp}$ are correlated due to secular spin-resonant interactions in the post Newtonian regime. [54–58] (something not accounted for in Table IX). One consequence of this alignment is that there is a tendency to drive the in-plane spin towards alignment or counter-alignment [54]. To model these effects, we examine how the recoil probabilities are modified if we assume the two extreme cases of alignment/counteralignment $\vec{S}_{1\perp} \propto \pm\vec{S}_{2\perp}$ of the in-plane component of the spins. Results from these studies are given in Table X. From the table, we can see that alignment ($\vec{S}_{1\perp} \propto -\vec{S}_{2\perp}$) suppresses large recoils by a factor of about 4, while counteralignment ($\vec{S}_{1\perp} \propto \vec{S}_{2\perp}$) increases the probability of large recoils by a factor of 2-3.

By examining the N configuration (which have non-zero values for $S_\parallel$, $S_\perp$, $\Delta_\parallel$, and $\Delta_\perp$), we found a new nonlinear term that amplifies the recoil. We verified this new effect by examining several other configurations (S, K, L). Since the N configurations are generic, in that all relevant spin parameters are non-trivial, it *appears* to be the case that there is no other large nonlinear contribution to the recoil for equal-mass BHBs. On the other hand, the unequal-mass regime, which is the subject of a major research effort by the authors, promises to hold many new surprises.

TABLE IX: Comparison between the predicted probabilities for a recoil in a given range as from the *hangup kick* and *cross kick* formulas for hot (top) and cold (middle) accretion and dry mergers (bottom).

Range	P(cross)	P(cross obs)	P(hang)	P(hang obs)
0-500	77.000%	91.301%	80.871%	93.210%
500-1000	15.564%	6.903%	13.843%	5.623%
1000-2000	6.930%	1.741%	5.046%	1.143%
2000-3000	0.498%	0.055%	0.237%	0.025%
3000-4000	0.007%	$3.5 \cdot 10^{-4}$%	0.003%	10^{-4}%
0-500	91.193%	97.765%	93.657%	98.522%
500-1000	7.974%	2.114%	5.919%	1.423%
1000-2000	0.832%	0.120%	0.423%	0.055%
2000-3000	0.002%	$1.3 \cdot 10^{-4}$%	$4.7 \cdot 10^{-4}$%	0 %
3000-4000	0%	0%	0%	0%
0-500	68.315%	86.465%	70.229%	87.693%
500-1000	18.382%	9.886%	18.157%	9.251%
1000-2000	11.820%	3.467%	10.519%	2.924%
2000-3000	1.449%	0.180%	1.074%	0.130 %
3000-4000	0.034%	0.002%	0.021%	0.001%

TABLE X: Comparison between the predicted probabilities for a recoil in a given range as from the *cross kick* formulas for hot (top) and cold (bottom) accretion when the in-plane components of the spins are forced to be aligned, antialigned, or are uncorrelated.

Range	P(aligned)	P(uncorrelated)	P(antialigned)
0-500	84.8855%	76.9754%	71.3786%
500-1000	11.2354%	15.5831%	17.6142%
1000-2000	3.7530%	6.9365%	9.9052%
2000-3000	0.1261%	0.4978%	1.0720%
3000-4000	0.0000%	0.0072%	0.0300%
0-500	95.3182%	91.1816%	87.0390%
500-1000	4.3465%	7.9853%	11.4147%
1000-2000	0.3348%	0.8309%	1.5400%
2000-3000	0.0005%	0.0022%	0.0064%
3000-4000	0.0000%	0.0000%	0.0000%

Acknowledgments

The authors thank M. Kesden for discussion on how PN dynamics modify spin distributions and recoils. M.Campanelli and H.Nakano for other discussions and J.Whelan for Eq. (8). The authors gratefully acknowledge the NSF for financial support from Grants AST-1028087, PHY-0929114, PHY-0969855, PHY-0903782, OCI-0832606, and DRL-1136221, and NASA for financial support from NASA Grant No. 07-ATFP07-0158. Computational resources were provided by the Ranger system at the Texas Advance Computing Center (XSEDE allocation TG-PHY060027N), which is supported in part by the NSF, and by NewHorizons at Rochester Institute of Technology, which was supported by NSF grant No. PHY-0722703, DMS-0820923 and AST-1028087.

Appendix A: Progenitor and Remnant Parameters

The tables in this appendix provide useful information for modeling remnant properties and how they relate to the configuration of the progenitor BHB. These results can be used to improve, both quantitatively and qualitatively, the empirical formulas that describe the remnant mass and spin [27, 59]. They can also be used in the construction of alternative formulas to model recoil velocities. Although we have been able to accurately model the off-plane recoil and make predictions that fit new runs, the formulas become increasingly complex to model higher nonlinear terms in the spins and one can seek a simpler, more compact formulation of the remnant recoil.

1. Initial Data parameters

TABLE XI: Initial data parameters. In all cases the puncture masses were chosen such that the total ADM mass of the binary was $1.0 \pm 10^{-6}M$. Here the punctures are located at $(x_{1,2}, 0, 0)$ with momenta $\pm(0, p, 0)$ and spins $\vec{S}_1 = (S_x, S_y, S_z)$. For the N configurations $\vec{S}_2 = 0$. The approximate initial eccentricities e_i, eccentricities measured over the last orbit e_f, and the number of orbits N, are also given.

CONF	m_{p1}/M	m_{p2}/M	x_1/M	x_2/M	p/M	S_x/M^2	S_y/M^2	S_z/M^2	m_{H1}	m_{H2}	$N_{e_f}^{e_i}$
NTH15PH0	0.307753	0.487740	4.077900	−4.307566	0.107293	0.000000	0.053084	0.198112	0.507321	0.504754	$4.5_{0.002}^{0.02}$
NTH15PH30	0.307762	0.487741	4.077900	−4.307566	0.107293	−0.026542	0.045972	0.198112	0.507322	0.504756	
NTH15PH60	0.307779	0.487745	4.077900	−4.307566	0.107293	−0.045972	0.026542	0.198112	0.507321	0.504759	
NTH15PH90	0.307786	0.487747	4.077900	−4.307566	0.107293	−0.053084	0.000000	0.198112	0.507321	0.504761	
NTH15PH120	0.307777	0.487745	4.077900	−4.307566	0.107293	−0.045972	−0.026542	0.198112	0.507319	0.504759	
NTH15PH150	0.307763	0.487741	4.077900	−4.307566	0.107293	−0.026542	−0.045972	0.198112	0.507321	0.504755	
NTH30PH0	0.307652	0.487705	4.098641	−4.304988	0.107491	0.000000	0.102538	0.177601	0.507291	0.504702	$4.5_{0.003}^{0.02}$
NTH30PH30	0.307686	0.487710	4.098641	−4.304988	0.107491	−0.051269	0.088800	0.177601	0.507293	0.504708	
NTH30PH60	0.307744	0.487725	4.098641	−4.304988	0.107491	−0.088800	0.051269	0.177601	0.507291	0.504721	
NTH30PH90	0.307775	0.487731	4.098641	−4.304988	0.107491	−0.102538	0.000000	0.177601	0.507288	0.504727	
NTH30PH120	0.307745	0.487725	4.098641	−4.304988	0.107491	−0.088800	−0.051269	0.177601	0.507287	0.504720	
NTH30PH150	0.307685	0.487711	4.098641	−4.304988	0.107491	−0.051269	−0.088800	0.177601	0.507289	0.504707	$4.5_{0.002}^{0.02}$
NTH45PH0	0.307512	0.487654	4.131521	−4.300556	0.107804	0.000000	0.144983	0.144983	0.507241	0.504625	
NTH45PH10	0.307522	0.487655	4.131521	−4.300556	0.107804	−0.025176	0.142780	0.144983	0.507244	0.504626	
NTH45PH20	0.307544	0.487659	4.131521	−4.300556	0.107804	−0.049587	0.136239	0.144983	0.507244	0.504631	
NTH45PH30	0.307584	0.487664	4.131521	−4.300556	0.107804	−0.072491	0.125559	0.144983	0.507246	0.504635	
NTH45PH40	0.307615	0.487676	4.131521	−4.300556	0.107804	−0.093193	0.111063	0.144983	0.507242	0.504647	
NTH45PH45	0.307636	0.487681	4.131521	−4.300556	0.107804	−0.102518	0.102518	0.144983	0.507242	0.504651	
NTH45PH50	0.307658	0.487685	4.131521	−4.300556	0.107804	−0.111063	0.093193	0.144983	0.507241	0.504655	
NTH45PH60	0.307700	0.487693	4.131521	−4.300556	0.107804	−0.125559	0.072491	0.144983	0.507240	0.504663	
NTH45PH75	0.307746	0.487703	4.131521	−4.300556	0.107804	−0.140042	0.037524	0.144983	0.507238	0.504671	
NTH45PH90	0.307757	0.487708	4.131521	−4.300556	0.107804	−0.144983	0.000000	0.144983	0.507233	0.504675	
NTH45PH975	0.307755	0.487707	4.131521	−4.300556	0.107804	−0.143742	−0.018924	0.144983	0.507233	0.504673	
NTH45PH120	0.307699	0.487694	4.131521	−4.300556	0.107804	−0.125559	−0.072491	0.144983	0.507230	0.504660	
NTH45PH1125	0.307723	0.487700	4.131521	−4.300556	0.107804	−0.133947	−0.055482	0.144983	0.507229	0.504666	
NTH45PH1275	0.307668	0.487688	4.131521	−4.300556	0.107804	−0.115022	−0.088260	0.144983	0.507229	0.504655	
NTH45PH150	0.307581	0.487665	4.131521	−4.300556	0.107804	−0.072491	−0.125559	0.144983	0.507236	0.504634	
NTH60PH0	0.307374	0.487595	4.174170	−4.294196	0.108211	0.000000	0.177524	0.102493	0.507180	0.504534	$4_{0.003}^{0.02}$
NTH60PH30	0.307465	0.487616	4.174170	−4.294196	0.108211	−0.088762	0.153740	0.102493	0.507184	0.504556	
NTH60PH60	0.307656	0.487656	4.174170	−4.294196	0.108211	−0.153740	0.088762	0.102493	0.507180	0.504592	
NTH60PH90	0.307743	0.487679	4.174170	−4.294196	0.108211	−0.177524	0.000000	0.102493	0.507170	0.504611	
NTH60PH120	0.307652	0.487657	4.174170	−4.294196	0.108211	−0.153740	−0.088762	0.102493	0.507164	0.504589	
NTH60PH150	0.307465	0.487617	4.174170	−4.294196	0.108211	−0.088762	−0.153740	0.102493	0.507169	0.504552	
NTH120PH0	0.307974	0.488280	4.661137	−4.542010	0.105032	0.000000	0.177129	−0.102265	0.506644	0.504014	$3.5_{0.004}^{0.02}$
NTH120PH30	0.308059	0.488303	4.661137	−4.542010	0.105032	−0.088564	0.153398	−0.102265	0.506646	0.504037	
NTH120PH60	0.308241	0.488342	4.661137	−4.542010	0.105032	−0.153398	0.088564	−0.102265	0.506642	0.504073	
NTH120PH90	0.308327	0.488364	4.661137	−4.542010	0.105032	−0.177129	0.000000	−0.102265	0.506634	0.504090	
NTH120PH120	0.308241	0.488342	4.661137	−4.542010	0.105032	−0.153398	−0.088564	−0.102265	0.506630	0.504068	
NTH120PH150	0.308058	0.488303	4.661137	−4.542010	0.105032	−0.088564	−0.153398	−0.102265	0.506635	0.504032	
NTH135PH0	0.308101	0.488288	4.701321	−4.532307	0.105392	0.000000	0.144599	−0.144599	0.506603	0.504004	$3.5_{0.004}^{0.02}$
NTH135PH30	0.308159	0.488302	4.701321	−4.532307	0.105392	−0.072299	0.125226	−0.144599	0.506602	0.504019	
NTH135PH60	0.308281	0.488329	4.701321	−4.532307	0.105392	−0.125226	0.072299	−0.144599	0.506600	0.504043	
NTH135PH90	0.308342	0.488343	4.701321	−4.532307	0.105392	−0.144599	0.000000	−0.144599	0.506597	0.504053	
NTH135PH120	0.308282	0.488329	4.701321	−4.532307	0.105392	−0.125226	−0.072299	−0.144599	0.506591	0.504039	
NTH135PH150	0.308161	0.488301	4.701321	−4.532307	0.105392	−0.072299	−0.125226	−0.144599	0.506595	0.504014	
NTH165PH0	0.308524	0.488582	4.854936	−4.625367	0.104087	0.000000	0.052895	−0.197408	0.506462	0.503917	$3.5_{0.005}^{0.02}$
NTH165PH30	0.308529	0.488584	4.854936	−4.625367	0.104087	−0.026448	0.045809	−0.197408	0.506461	0.503920	
NTH165PH60	0.308549	0.488587	4.854936	−4.625367	0.104087	−0.045809	0.026448	−0.197408	0.506463	0.503922	
NTH165PH90	0.308553	0.488590	4.854936	−4.625367	0.104087	−0.052895	0.000000	−0.197408	0.506461	0.503925	
NTH165PH120	0.308545	0.488588	4.854936	−4.625367	0.104087	−0.045809	−0.026448	−0.197408	0.506461	0.503923	
NTH165PH150	0.308529	0.488584	4.854936	−4.625367	0.104087	−0.026448	−0.045809	−0.197408	0.506460	0.503919	

TABLE XII: Initial data parameters. In all cases the puncture masses were chosen such that the total ADM mass of the binary was $1.0 \pm 10^{-6}M$. Here the punctures are located at $(x_{1,2}, 0, 0)$ with momenta $\pm(0, p, 0)$ and spins $\vec{S}_1 = (S_x, S_y, S_z)$. For the S configurations the second BH spin is given by $\vec{S}_2 = -\vec{S}_1$, while for the K configurations it is given by $\vec{S}_2 = (S_x, S_y, -S_z)$. Finally, for the L configurations, $\vec{S}_2 = (0, 0, |\vec{S}_1|)$. The approximate initial eccentricities e_i, eccentricities measured over the last orbit e_f, and the number of orbits N, are also given.

CONF	m_{p1}/M	m_{p2}/M	x_1/M	x_2/M	p/M	S_x/M^2	S_y/M^2	S_z/M^2	m_{H1}	m_{H2}	$N_{e_f}^{e_i}$
STH45PH0	0.302923	0.303004	4.194252	−4.534000	0.107508	0.000000	0.144813	0.144813	0.505422	0.505411	$3.5^{0.02}_{0.004}$
STH45PH30	0.303051	0.303137	4.194252	−4.534000	0.107508	−0.072406	0.125412	0.144813	0.505446	0.505436	
STH45PH60	0.303313	0.303398	4.194252	−4.534000	0.107508	−0.125412	0.072406	0.144813	0.505482	0.505474	
STH45PH90	0.303442	0.303531	4.194252	−4.534000	0.107508	−0.144813	0.000000	0.144813	0.505496	0.505488	
STH45PH120	0.303312	0.303400	4.194252	−4.534000	0.107508	−0.125412	−0.072406	0.144813	0.505468	0.505461	
STH45PH150	0.303051	0.303137	4.194252	−4.534000	0.107508	−0.072406	−0.125412	0.144813	0.505433	0.505424	
KTH45PH0	0.303010	0.303092	4.187859	−4.527100	0.107491	0.000000	0.144822	0.144822	0.505460	0.505454	$3.5^{0.02}_{0.004}$
KTH45PH30	0.303090	0.303173	4.187859	−4.527100	0.107491	−0.072411	0.125419	0.144822	0.505469	0.505459	
KTH45PH60	0.303250	0.303335	4.187859	−4.527100	0.107491	−0.125419	0.072411	0.144822	0.505474	0.505464	
KTH45PH90	0.303330	0.303416	4.187859	−4.527100	0.107491	−0.144822	0.000000	0.144822	0.505471	0.505465	
KTH45PH105	0.303310	0.303393	4.187859	−4.527100	0.107491	−0.139887	−0.037483	0.144822	0.505466	0.505462	
KTH45PH120	0.303249	0.303336	4.187859	−4.527100	0.107491	−0.125419	−0.072411	0.144822	0.505460	0.505458	
KTH45PH135	0.303171	0.303254	4.187859	−4.527100	0.107491	−0.102404	−0.102404	0.144822	0.505457	0.505454	
KTH45PH150	0.303091	0.303173	4.187859	−4.527100	0.107491	−0.072411	−0.125419	0.144822	0.505456	0.505452	
KTH45PH165	0.303028	0.303118	4.187859	−4.527100	0.107491	−0.037483	−0.139887	0.144822	0.505456	0.505454	
KTH45PH30	0.303090	0.303173	4.187859	−4.527100	0.107491	−0.072411	0.125419	0.144822	0.505469	0.505459	
KTH45PH60	0.303250	0.303335	4.187859	−4.527100	0.107491	−0.125419	0.072411	0.144822	0.505474	0.505464	
KTH45PH90	0.303330	0.303416	4.187859	−4.527100	0.107491	−0.144822	0.000000	0.144822	0.505471	0.505465	
KTH45PH120	0.303249	0.303336	4.187859	−4.527100	0.107491	−0.125419	−0.072411	0.144822	0.505460	0.505458	
KTH45PH150	0.303091	0.303173	4.187859	−4.527100	0.107491	−0.072411	−0.125419	0.144822	0.505456	0.505452	
KTH22.5PH0	0.303316	0.303422	4.133612	−4.576616	0.107486	0.000000	0.078379	0.189223	0.505509	0.505497	
KTH22.5PH30	0.303338	0.303447	4.133612	−4.576616	0.107486	−0.039189	0.067878	0.189223	0.505512	0.505500	
KTH22.5PH60	0.303385	0.303494	4.133612	−4.576616	0.107486	−0.067878	0.039189	0.189223	0.505514	0.505502	
KTH22.5PH90	0.303406	0.303520	4.133612	−4.576616	0.107486	−0.078379	0.000000	0.189223	0.505512	0.505503	
KTH22.5PH120	0.303384	0.303495	4.133612	−4.576616	0.107486	−0.067878	−0.039189	0.189223	0.505510	0.505501	
KTH22.5PH150	0.303336	0.303449	4.133612	−4.576616	0.107486	−0.039189	−0.067878	0.189223	0.505508	0.505499	
LPH0	0.302983	0.303118	4.400426	−4.164556	0.105611	0.000000	0.205015	0.000000	0.505728	0.505627	$5^{0.02}_{0.005}$
LPH30	0.303110	0.303193	4.400426	−4.164556	0.105611	−0.102508	0.177549	0.000000	0.505737	0.505652	
LPH60	0.303359	0.303348	4.400426	−4.164556	0.105611	−0.177549	0.102508	0.000000	0.505732	0.505703	
LPH90	0.303478	0.303430	4.400426	−4.164556	0.105611	−0.205015	0.000000	0.000000	0.505722	0.505727	
LPH120	0.303361	0.303345	4.400426	−4.164556	0.105611	−0.177549	−0.102508	0.000000	0.505720	0.505699	
LPH150	0.303111	0.303193	4.400426	−4.164556	0.105611	−0.102508	−0.177549	0.000000	0.505722	0.505649	
N9TH55PH0	0.202809	0.485667	4.144277	−4.298725	0.107926	0.000000	0.188937	0.132295	0.508839	0.502637	$4.5^{0.02}_{0.006}$
N9TH55PH30	0.202990	0.485691	4.144277	−4.298725	0.107926	−0.094468	0.163624	0.132295	0.508843	0.502662	
N9TH55PH60	0.203344	0.485745	4.144277	−4.298725	0.107926	−0.163624	0.094468	0.132295	0.508839	0.502712	
N9TH55PH90	0.203494	0.485777	4.144277	−4.298725	0.107926	−0.188937	0.000000	0.132295	0.508828	0.502738	
N9TH55PH150	0.202992	0.485690	4.144277	−4.298725	0.107926	−0.094468	−0.163624	0.132295	0.508828	0.502655	

2. Remnant Properties and Radiated Energy-Momentum

TABLE XIII: Remnant horizon properties using the IH formalism. Quoted errors are calculated from the variation of IH quantities with time. See Tables XVII and XVIII for more realistic measures of the true error.

CONF	m_H/M	α	S_x/M	S_y/M	S_z/M
NTH15PH0	$0.949002 \pm 2.5 \cdot 10^{-5}$	$0.800400 \pm 2.9 \cdot 10^{-5}$	$-0.0059188 \pm 5 \cdot 10^{-3}$	$0.0229940 \pm 5 \cdot 10^{-3}$	$0.72045 \pm 3 \cdot 10^{-4}$
NTH15PH30	$0.949096 \pm 2.5 \cdot 10^{-5}$	$0.800619 \pm 3.1 \cdot 10^{-5}$	$-0.0087750 \pm 5 \cdot 10^{-7}$	$0.0327727 \pm 2 \cdot 10^{-6}$	$0.72039 \pm 4 \cdot 10^{-5}$
NTH15PH60	$0.949177 \pm 2.5 \cdot 10^{-5}$	$0.800721 \pm 2.8 \cdot 10^{-5}$	$-0.0193710 \pm 1 \cdot 10^{-6}$	$0.0200562 \pm 1 \cdot 10^{-6}$	$0.72086 \pm 4 \cdot 10^{-5}$
NTH15PH90	$0.949169 \pm 2.6 \cdot 10^{-5}$	$0.800619 \pm 3.4 \cdot 10^{-5}$	$-0.0247011 \pm 5 \cdot 10^{-4}$	$0.0037424 \pm 2 \cdot 10^{-3}$	$0.72086 \pm 4 \cdot 10^{-5}$
NTH15PH120	$0.949076 \pm 2.6 \cdot 10^{-5}$	$0.800397 \pm 3.3 \cdot 10^{-5}$	$-0.0231286 \pm 1 \cdot 10^{-2}$	$-0.0123739 \pm 7 \cdot 10^{-3}$	$0.72048 \pm 4 \cdot 10^{-4}$
NTH15PH150	$0.948988 \pm 2.5 \cdot 10^{-5}$	$0.800289 \pm 2.9 \cdot 10^{-5}$	$-0.0271884 \pm 1 \cdot 10^{-2}$	$-0.0324823 \pm 7 \cdot 10^{-3}$	$0.71948 \pm 1 \cdot 10^{-3}$
NTH30PH0	$0.950352 \pm 1.1 \cdot 10^{-5}$	$0.793089 \pm 8.7 \cdot 10^{-6}$	$0.0102968 \pm 3 \cdot 10^{-7}$	$0.0606032 \pm 2 \cdot 10^{-6}$	$0.71365 \pm 2 \cdot 10^{-5}$
NTH30PH30	$0.950660 \pm 1.0 \cdot 10^{-5}$	$0.793625 \pm 1.1 \cdot 10^{-5}$	$-0.0433712 \pm 6 \cdot 10^{-7}$	$0.0612195 \pm 8 \cdot 10^{-7}$	$0.71331 \pm 1 \cdot 10^{-5}$
NTH30PH60	$0.950722 \pm 1.1 \cdot 10^{-5}$	$0.793366 \pm 1.9 \cdot 10^{-5}$	$-0.0469123 \pm 7 \cdot 10^{-7}$	$0.0326284 \pm 5 \cdot 10^{-7}$	$0.71482 \pm 2 \cdot 10^{-5}$
NTH30PH90	$0.950488 \pm 1.3 \cdot 10^{-5}$	$0.792563 \pm 1.2 \cdot 10^{-5}$	$-0.0599863 \pm 1 \cdot 10^{-6}$	$0.0046845 \pm 2 \cdot 10^{-7}$	$0.71349 \pm 2 \cdot 10^{-5}$
NTH30PH120	$0.950142 \pm 1.2 \cdot 10^{-5}$	$0.791909 \pm 9.2 \cdot 10^{-6}$	$-0.0680924 \pm 2 \cdot 10^{-6}$	$-0.0250607 \pm 8 \cdot 10^{-7}$	$0.71122 \pm 3 \cdot 10^{-5}$
NTH30PH150	$0.950063 \pm 9.9 \cdot 10^{-6}$	$0.792167 \pm 1.2 \cdot 10^{-5}$	$-0.0279134 \pm 1 \cdot 10^{-6}$	$-0.0566108 \pm 2 \cdot 10^{-6}$	$0.71223 \pm 3 \cdot 10^{-5}$
NTH45PH0	$0.952965 \pm 4.2 \cdot 10^{-6}$	$0.781452 \pm 1.8 \cdot 10^{-5}$	$0.0052411 \pm 2 \cdot 10^{-7}$	$0.0862119 \pm 2 \cdot 10^{-6}$	$0.70439 \pm 2 \cdot 10^{-5}$
NTH45PH10	$0.952963 \pm 5.0 \cdot 10^{-6}$	$0.781286 \pm 2.4 \cdot 10^{-5}$	$-0.0068446 \pm 3 \cdot 10^{-7}$	$0.1028876 \pm 3 \cdot 10^{-6}$	$0.70198 \pm 3 \cdot 10^{-5}$
NTH45PH20	$0.952898 \pm 5.0 \cdot 10^{-6}$	$0.780915 \pm 2.7 \cdot 10^{-5}$	$-0.0280650 \pm 9 \cdot 10^{-7}$	$0.0982404 \pm 3 \cdot 10^{-6}$	$0.70168 \pm 3 \cdot 10^{-5}$
NTH45PH30	$0.952788 \pm 3.9 \cdot 10^{-6}$	$0.780408 \pm 2.5 \cdot 10^{-5}$	$-0.0396175 \pm 1 \cdot 10^{-6}$	$0.0727714 \pm 2 \cdot 10^{-6}$	$0.70360 \pm 3 \cdot 10^{-5}$
NTH45PH40	$0.952657 \pm 3.7 \cdot 10^{-6}$	$0.779872 \pm 2.4 \cdot 10^{-5}$	$-0.0573442 \pm 2 \cdot 10^{-6}$	$0.0647666 \pm 2 \cdot 10^{-6}$	$0.70247 \pm 2 \cdot 10^{-5}$
NTH45PH45	$0.952594 \pm 4.0 \cdot 10^{-6}$	$0.779622 \pm 2.8 \cdot 10^{-5}$	$-0.0611883 \pm 2 \cdot 10^{-6}$	$0.0605063 \pm 2 \cdot 10^{-6}$	$0.70220 \pm 3 \cdot 10^{-5}$
NTH45PH50	$0.952517 \pm 5.1 \cdot 10^{-6}$	$0.779337 \pm 3.3 \cdot 10^{-5}$	$-0.0622867 \pm 2 \cdot 10^{-6}$	$0.0533615 \pm 2 \cdot 10^{-6}$	$0.70231 \pm 3 \cdot 10^{-5}$
NTH45PH60	$0.952371 \pm 5.5 \cdot 10^{-6}$	$0.778824 \pm 3.5 \cdot 10^{-5}$	$-0.0819302 \pm 4 \cdot 10^{-6}$	$0.0635694 \pm 3 \cdot 10^{-6}$	$0.69875 \pm 4 \cdot 10^{-5}$
NTH45PH75	$0.952129 \pm 5.7 \cdot 10^{-6}$	$0.778112 \pm 4.3 \cdot 10^{-5}$	$-0.0837902 \pm 4 \cdot 10^{-6}$	$0.0188236 \pm 9 \cdot 10^{-7}$	$0.70015 \pm 4 \cdot 10^{-5}$
NTH45PH90	$0.951927 \pm 8.6 \cdot 10^{-6}$	$0.777677 \pm 5.0 \cdot 10^{-5}$	$-0.0926429 \pm 5 \cdot 10^{-6}$	$0.0144582 \pm 9 \cdot 10^{-7}$	$0.69844 \pm 5 \cdot 10^{-5}$
NTH45PH975	$0.951866 \pm 6.8 \cdot 10^{-6}$	$0.777638 \pm 5.1 \cdot 10^{-5}$	$-0.0940831 \pm 6 \cdot 10^{-6}$	$-0.0000789 \pm 5 \cdot 10^{-8}$	$0.69827 \pm 5 \cdot 10^{-5}$
NTH45PH120	$0.951917 \pm 7.5 \cdot 10^{-6}$	$0.778302 \pm 5.8 \cdot 10^{-5}$	$-0.0863067 \pm 6 \cdot 10^{-6}$	$-0.0311843 \pm 2 \cdot 10^{-6}$	$0.69926 \pm 5 \cdot 10^{-5}$
NTH45PH1125	$0.951859 \pm 6.0 \cdot 10^{-6}$	$0.777949 \pm 5.2 \cdot 10^{-5}$	$-0.0884714 \pm 5 \cdot 10^{-6}$	$-0.0238097 \pm 1 \cdot 10^{-6}$	$0.69887 \pm 5 \cdot 10^{-5}$
NTH45PH1275	$0.952012 \pm 5.3 \cdot 10^{-6}$	$0.778733 \pm 4.8 \cdot 10^{-5}$	$-0.0813575 \pm 5 \cdot 10^{-6}$	$-0.0424656 \pm 3 \cdot 10^{-6}$	$0.69979 \pm 5 \cdot 10^{-5}$
NTH45PH150	$0.952488 \pm 4.1 \cdot 10^{-6}$	$0.780369 \pm 2.3 \cdot 10^{-5}$	$-0.0509898 \pm 2 \cdot 10^{-6}$	$-0.0707933 \pm 2 \cdot 10^{-6}$	$0.70258 \pm 3 \cdot 10^{-5}$
NTH60PH0	$0.954548 \pm 9.4 \cdot 10^{-6}$	$0.759903 \pm 3.6 \cdot 10^{-5}$	$0.0120181 \pm 6 \cdot 10^{-7}$	$0.1059528 \pm 5 \cdot 10^{-6}$	$0.68413 \pm 3 \cdot 10^{-5}$
NTH60PH30	$0.954117 \pm 8.1 \cdot 10^{-6}$	$0.758701 \pm 3.8 \cdot 10^{-5}$	$-0.0608939 \pm 2 \cdot 10^{-6}$	$0.1016092 \pm 4 \cdot 10^{-6}$	$0.68044 \pm 3 \cdot 10^{-5}$
NTH60PH60	$0.954263 \pm 8.3 \cdot 10^{-6}$	$0.758808 \pm 4.0 \cdot 10^{-5}$	$-0.1015464 \pm 4 \cdot 10^{-6}$	$0.0580071 \pm 2 \cdot 10^{-6}$	$0.68102 \pm 3 \cdot 10^{-5}$
NTH60PH90	$0.954825 \pm 9.1 \cdot 10^{-6}$	$0.760276 \pm 1.9 \cdot 10^{-5}$	$-0.1254426 \pm 4 \cdot 10^{-6}$	$-0.0000259 \pm 5 \cdot 10^{-8}$	$0.68169 \pm 3 \cdot 10^{-5}$
NTH60PH120	$0.955661 \pm 5.2 \cdot 10^{-6}$	$0.762668 \pm 2.3 \cdot 10^{-5}$	$-0.0923975 \pm 2 \cdot 10^{-6}$	$-0.0521792 \pm 1 \cdot 10^{-6}$	$0.68841 \pm 2 \cdot 10^{-5}$
NTH60PH150	$0.955595 \pm 5.8 \cdot 10^{-6}$	$0.762609 \pm 1.9 \cdot 10^{-5}$	$-0.0525913 \pm 9 \cdot 10^{-7}$	$-0.1010084 \pm 2 \cdot 10^{-6}$	$0.68701 \pm 2 \cdot 10^{-5}$
NTH120PH0	$0.965664 \pm 3.6 \cdot 10^{-6}$	$0.644178 \pm 8.9 \cdot 10^{-6}$	$-0.0196764 \pm 3 \cdot 10^{-7}$	$0.1049745 \pm 2 \cdot 10^{-6}$	$0.59113 \pm 1 \cdot 10^{-5}$
NTH120PH30	$0.965986 \pm 3.5 \cdot 10^{-6}$	$0.644558 \pm 8.9 \cdot 10^{-6}$	$-0.0503997 \pm 7 \cdot 10^{-7}$	$0.0898719 \pm 1 \cdot 10^{-6}$	$0.59256 \pm 1 \cdot 10^{-5}$
NTH120PH60	$0.965901 \pm 3.7 \cdot 10^{-6}$	$0.643317 \pm 8.3 \cdot 10^{-6}$	$-0.1022275 \pm 1 \cdot 10^{-6}$	$0.0432199 \pm 6 \cdot 10^{-7}$	$0.58984 \pm 1 \cdot 10^{-5}$
NTH120PH90	$0.965596 \pm 4.6 \cdot 10^{-6}$	$0.641770 \pm 8.5 \cdot 10^{-6}$	$-0.1096112 \pm 1 \cdot 10^{-6}$	$-0.0101321 \pm 2 \cdot 10^{-7}$	$0.58816 \pm 1 \cdot 10^{-5}$
NTH120PH120	$0.965027 \pm 4.3 \cdot 10^{-6}$	$0.640323 \pm 1.2 \cdot 10^{-5}$	$-0.0745858 \pm 1 \cdot 10^{-6}$	$-0.0501520 \pm 8 \cdot 10^{-7}$	$0.58951 \pm 1 \cdot 10^{-5}$
NTH120PH150	$0.965083 \pm 3.5 \cdot 10^{-6}$	$0.641861 \pm 1.1 \cdot 10^{-5}$	$-0.0473661 \pm 8 \cdot 10^{-7}$	$-0.0969227 \pm 2 \cdot 10^{-6}$	$0.58801 \pm 1 \cdot 10^{-5}$
NTH135PH0	$0.967523 \pm 4.8 \cdot 10^{-6}$	$0.611243 \pm 1.4 \cdot 10^{-5}$	$-0.0111685 \pm 2 \cdot 10^{-7}$	$0.0886077 \pm 2 \cdot 10^{-6}$	$0.56517 \pm 2 \cdot 10^{-5}$
NTH135PH30	$0.967277 \pm 3.8 \cdot 10^{-6}$	$0.609924 \pm 7.9 \cdot 10^{-6}$	$-0.0536160 \pm 8 \cdot 10^{-7}$	$0.0687996 \pm 1 \cdot 10^{-6}$	$0.56395 \pm 1 \cdot 10^{-5}$
NTH135PH60	$0.967256 \pm 4.0 \cdot 10^{-6}$	$0.609695 \pm 9.3 \cdot 10^{-6}$	$-0.0842716 \pm 1 \cdot 10^{-6}$	$0.0381523 \pm 6 \cdot 10^{-7}$	$0.56287 \pm 1 \cdot 10^{-5}$
NTH135PH90	$0.967402 \pm 4.4 \cdot 10^{-6}$	$0.610218 \pm 1.0 \cdot 10^{-5}$	$-0.0831299 \pm 1 \cdot 10^{-6}$	$-0.0206110 \pm 4 \cdot 10^{-7}$	$0.56462 \pm 1 \cdot 10^{-5}$
NTH135PH120	$0.967739 \pm 3.5 \cdot 10^{-6}$	$0.611715 \pm 8.3 \cdot 10^{-6}$	$-0.0587466 \pm 9 \cdot 10^{-7}$	$-0.0630778 \pm 1 \cdot 10^{-6}$	$0.56636 \pm 1 \cdot 10^{-5}$
NTH135PH150	$0.967820 \pm 3.7 \cdot 10^{-6}$	$0.612348 \pm 1.0 \cdot 10^{-5}$	$-0.0352962 \pm 6 \cdot 10^{-7}$	$-0.0865760 \pm 1 \cdot 10^{-6}$	$0.56590 \pm 1 \cdot 10^{-5}$
NTH165PH0	$0.969939 \pm 4.2 \cdot 10^{-6}$	$0.566054 \pm 1.0 \cdot 10^{-5}$	$-0.0143038 \pm 3 \cdot 10^{-7}$	$0.0238197 \pm 4 \cdot 10^{-7}$	$0.53181 \pm 1 \cdot 10^{-5}$
NTH165PH30	$0.969916 \pm 3.5 \cdot 10^{-6}$	$0.565949 \pm 9.5 \cdot 10^{-6}$	$-0.0157146 \pm 3 \cdot 10^{-7}$	$0.0275530 \pm 5 \cdot 10^{-7}$	$0.53146 \pm 1 \cdot 10^{-5}$
NTH165PH60	$0.969934 \pm 3.9 \cdot 10^{-6}$	$0.565965 \pm 9.7 \cdot 10^{-6}$	$-0.0247061 \pm 4 \cdot 10^{-7}$	$0.0148809 \pm 3 \cdot 10^{-7}$	$0.53166 \pm 1 \cdot 10^{-5}$
NTH165PH90	$0.969973 \pm 4.5 \cdot 10^{-6}$	$0.566113 \pm 9.6 \cdot 10^{-6}$	$-0.0399334 \pm 6 \cdot 10^{-7}$	$-0.0092692 \pm 2 \cdot 10^{-7}$	$0.53105 \pm 1 \cdot 10^{-5}$
NTH165PH120	$0.969995 \pm 4.3 \cdot 10^{-6}$	$0.566233 \pm 8.5 \cdot 10^{-6}$	$-0.0282134 \pm 5 \cdot 10^{-7}$	$-0.0310082 \pm 5 \cdot 10^{-7}$	$0.53111 \pm 1 \cdot 10^{-5}$
NTH165PH150	$0.969978 \pm 5.1 \cdot 10^{-6}$	$0.566194 \pm 8.8 \cdot 10^{-6}$	$-0.0058152 \pm 1 \cdot 10^{-7}$	$-0.0245145 \pm 4 \cdot 10^{-7}$	$0.53211 \pm 1 \cdot 10^{-5}$

TABLE XIV: Remnant horizon properties using the IH formalism (continued). Quoted errors are calculated from the variation of IH quantities with time. See Tables XVII and XVIII for more realistic measures of the true error.

CONF	m_H/M	α	S_x/M	S_y/M	S_z/M
STH45PH0	$0.960386 \pm 1.2 \cdot 10^{-5}$	$0.681328 \pm 5.5 \cdot 10^{-5}$	$-0.0029258 \pm 2 \cdot 10^{-7}$	$-0.0112825 \pm 7 \cdot 10^{-7}$	$0.62831 \pm 4 \cdot 10^{-5}$
STH45PH30	$0.961370 \pm 1.1 \cdot 10^{-5}$	$0.683685 \pm 3.8 \cdot 10^{-5}$	$-0.0049041 \pm 2 \cdot 10^{-7}$	$-0.0106043 \pm 4 \cdot 10^{-7}$	$0.63178 \pm 3 \cdot 10^{-5}$
STH45PH60	$0.961447 \pm 1.2 \cdot 10^{-5}$	$0.682989 \pm 4.3 \cdot 10^{-5}$	$-0.0059768 \pm 3 \cdot 10^{-7}$	$-0.0059344 \pm 3 \cdot 10^{-7}$	$0.63128 \pm 3 \cdot 10^{-5}$
STH45PH90	$0.960884 \pm 1.3 \cdot 10^{-5}$	$0.680984 \pm 5.8 \cdot 10^{-5}$	$0.0043894 \pm 3 \cdot 10^{-7}$	$0.0118551 \pm 7 \cdot 10^{-7}$	$0.62862 \pm 4 \cdot 10^{-5}$
STH45PH120	$0.960038 \pm 1.5 \cdot 10^{-5}$	$0.678902 \pm 5.9 \cdot 10^{-5}$	$-0.0020680 \pm 2 \cdot 10^{-7}$	$-0.0083257 \pm 6 \cdot 10^{-7}$	$0.62567 \pm 4 \cdot 10^{-5}$
STH45PH150	$0.959700 \pm 1.6 \cdot 10^{-5}$	$0.678717 \pm 6.1 \cdot 10^{-5}$	$-0.0006975 \pm 9 \cdot 10^{-8}$	$0.0130117 \pm 8 \cdot 10^{-7}$	$0.62498 \pm 4 \cdot 10^{-5}$
KTH45PH0	$0.959306 \pm 4.6 \cdot 10^{-6}$	$0.733285 \pm 1.5 \cdot 10^{-5}$	$0.0096842 \pm 3 \cdot 10^{-7}$	$0.1670485 \pm 4 \cdot 10^{-6}$	$0.65374 \pm 2 \cdot 10^{-5}$
KTH45PH30	$0.959031 \pm 4.6 \cdot 10^{-6}$	$0.731242 \pm 7.0 \cdot 10^{-6}$	$-0.0824495 \pm 1 \cdot 10^{-6}$	$0.1443256 \pm 2 \cdot 10^{-6}$	$0.65169 \pm 1 \cdot 10^{-5}$
KTH45PH60	$0.958963 \pm 4.3 \cdot 10^{-6}$	$0.729211 \pm 3.8 \cdot 10^{-5}$	$-0.1581502 \pm 7 \cdot 10^{-6}$	$0.0892345 \pm 4 \cdot 10^{-6}$	$0.64554 \pm 3 \cdot 10^{-5}$
KTH45PH90	$0.958292 \pm 6.6 \cdot 10^{-6}$	$0.727374 \pm 1.3 \cdot 10^{-5}$	$-0.1681021 \pm 4 \cdot 10^{-6}$	$-0.0020425 \pm 1 \cdot 10^{-7}$	$0.64646 \pm 2 \cdot 10^{-5}$
KTH45PH105	$0.957553 \pm 1.3 \cdot 10^{-5}$	$0.725788 \pm 4.7 \cdot 10^{-5}$	$-0.1589683 \pm 6 \cdot 10^{-6}$	$-0.0343141 \pm 1 \cdot 10^{-6}$	$0.64530 \pm 3 \cdot 10^{-5}$
KTH45PH120	$0.956969 \pm 7.6 \cdot 10^{-6}$	$0.724630 \pm 2.1 \cdot 10^{-5}$	$-0.1604927 \pm 3 \cdot 10^{-6}$	$-0.0888209 \pm 2 \cdot 10^{-6}$	$0.63775 \pm 2 \cdot 10^{-5}$
KTH45PH135	$0.957068 \pm 3.3 \cdot 10^{-6}$	$0.725770 \pm 1.3 \cdot 10^{-5}$	$-0.1359932 \pm 3 \cdot 10^{-6}$	$-0.1290310 \pm 3 \cdot 10^{-6}$	$0.63781 \pm 2 \cdot 10^{-5}$
KTH45PH150	$0.958008 \pm 3.9 \cdot 10^{-6}$	$0.729194 \pm 3.7 \cdot 10^{-5}$	$-0.0820269 \pm 4 \cdot 10^{-6}$	$-0.1513764 \pm 7 \cdot 10^{-6}$	$0.64671 \pm 3 \cdot 10^{-5}$
KTH45PH165	$0.958990 \pm 4.4 \cdot 10^{-6}$	$0.732376 \pm 2.2 \cdot 10^{-5}$	$-0.0389777 \pm 1 \cdot 10^{-6}$	$-0.1725190 \pm 5 \cdot 10^{-6}$	$0.64990 \pm 2 \cdot 10^{-5}$
KTH22.5PH0	$0.959881 \pm 5.2 \cdot 10^{-6}$	$0.695101 \pm 2.4 \cdot 10^{-5}$	$-0.0103440 \pm 3 \cdot 10^{-7}$	$0.0872087 \pm 2 \cdot 10^{-6}$	$0.63440 \pm 2 \cdot 10^{-5}$
KTH22.5PH30	$0.959651 \pm 6.5 \cdot 10^{-6}$	$0.694469 \pm 2.8 \cdot 10^{-5}$	$-0.0551628 \pm 2 \cdot 10^{-6}$	$0.0763874 \pm 2 \cdot 10^{-6}$	$0.63258 \pm 2 \cdot 10^{-5}$
KTH22.5PH60	$0.959845 \pm 5.0 \cdot 10^{-6}$	$0.694970 \pm 1.8 \cdot 10^{-5}$	$-0.0860895 \pm 2 \cdot 10^{-6}$	$0.0396870 \pm 8 \cdot 10^{-7}$	$0.63322 \pm 2 \cdot 10^{-5}$
KTH22.5PH90	$0.960412 \pm 3.7 \cdot 10^{-6}$	$0.696387 \pm 1.6 \cdot 10^{-5}$	$-0.0946340 \pm 2 \cdot 10^{-6}$	$-0.0085426 \pm 2 \cdot 10^{-7}$	$0.63527 \pm 2 \cdot 10^{-5}$
KTH22.5PH120	$0.960943 \pm 4.4 \cdot 10^{-6}$	$0.697710 \pm 1.9 \cdot 10^{-5}$	$-0.0768168 \pm 2 \cdot 10^{-6}$	$-0.0372213 \pm 9 \cdot 10^{-7}$	$0.63859 \pm 2 \cdot 10^{-5}$
KTH22.5PH150	$0.960575 \pm 4.8 \cdot 10^{-6}$	$0.696820 \pm 1.4 \cdot 10^{-5}$	$-0.0395611 \pm 6 \cdot 10^{-7}$	$-0.0746323 \pm 1 \cdot 10^{-6}$	$0.63739 \pm 1 \cdot 10^{-5}$
LPH0	$0.943756 \pm 2.4 \cdot 10^{-5}$	$0.815716 \pm 2.8 \cdot 10^{-4}$	$-0.0000661 \pm 8 \cdot 10^{-8}$	$0.1262529 \pm 5 \cdot 10^{-5}$	$0.71548 \pm 3 \cdot 10^{-4}$
LPH30	$0.943158 \pm 9.2 \cdot 10^{-6}$	$0.814545 \pm 4.7 \cdot 10^{-5}$	$-0.0688881 \pm 5 \cdot 10^{-6}$	$0.1112364 \pm 8 \cdot 10^{-6}$	$0.71266 \pm 6 \cdot 10^{-5}$
LPH60	$0.943272 \pm 2.1 \cdot 10^{-5}$	$0.814734 \pm 3.1 \cdot 10^{-4}$	$-0.1118922 \pm 5 \cdot 10^{-5}$	$0.0791998 \pm 3 \cdot 10^{-5}$	$0.71184 \pm 3 \cdot 10^{-4}$
LPH90	$0.944022 \pm 2.2 \cdot 10^{-5}$	$0.816420 \pm 3.4 \cdot 10^{-4}$	$-0.1400266 \pm 6 \cdot 10^{-5}$	$-0.0082355 \pm 4 \cdot 10^{-6}$	$0.71393 \pm 3 \cdot 10^{-4}$
LPH120	$0.945434 \pm 2.6 \cdot 10^{-5}$	$0.819694 \pm 4.2 \cdot 10^{-4}$	$-0.1281539 \pm 7 \cdot 10^{-5}$	$-0.0585698 \pm 3 \cdot 10^{-5}$	$0.71900 \pm 4 \cdot 10^{-4}$
LPH150	$0.945209 \pm 1.8 \cdot 10^{-5}$	$0.818582 \pm 1.7 \cdot 10^{-4}$	$-0.0745095 \pm 2 \cdot 10^{-5}$	$-0.1087893 \pm 3 \cdot 10^{-5}$	$0.71935 \pm 2 \cdot 10^{-4}$
N9TH55PH0	$0.953186 \pm 4.3 \times 10^{-6}$	$0.781970 \pm 1.1 \times 10^{-5}$	$0.0033146 \pm 8 \times 10^{-8}$	$0.1352916 \pm 1 \times 10^{-6}$	$0.69746 \pm 1 \times 10^{-5}$
N9TH55PH30	$0.952694 \pm 4.5 \times 10^{-6}$	$0.779882 \pm 1.2 \times 10^{-5}$	$-0.0534949 \pm 7 \times 10^{-7}$	$0.0979401 \pm 1 \times 10^{-6}$	$0.69899 \pm 1 \times 10^{-5}$
N9TH55PH60	$0.952068 \pm 3.7 \times 10^{-6}$	$0.777501 \pm 9.8 \times 10^{-6}$	$-0.1037737 \pm 2 \times 10^{-6}$	$0.0783538 \pm 1 \times 10^{-6}$	$0.69265 \pm 2 \times 10^{-5}$
N9TH55PH90	$0.951446 \pm 3.7 \times 10^{-6}$	$0.775873 \pm 1.7 \times 10^{-5}$	$-0.1194599 \pm 2 \times 10^{-6}$	$0.0157632 \pm 4 \times 10^{-7}$	$0.69195 \pm 2 \times 10^{-5}$
N9TH55PH150	$0.952695 \pm 4.1 \times 10^{-6}$	$0.781022 \pm 9.6 \times 10^{-6}$	$-0.0678230 \pm 1 \times 10^{-6}$	$-0.1105645 \pm 2 \times 10^{-6}$	$0.69691 \pm 1 \times 10^{-5}$

TABLE XV: Radiated mass, angular momentum, and the remnant recoil (in original frame) as calculated from ψ_4. Errors quoted are from differences between to extrapolation to $r=\infty$. See Tables XVII and XVIII for more accurate measurement of the error.

CONF	$\delta M_{\rm rad}$	δJ_x	δJ_y	δJ_z	V_x	V_y	V_z
NTH15PH0	0.0494 ± 0.0001	-0.0015 ± 0.0008	0.0199 ± 0.0023	0.3690 ± 0.0023	75 ± 22	113 ± 5	-456 ± 2
NTH15PH30	0.0493 ± 0.0001	-0.0090 ± 0.0004	0.0154 ± 0.0005	0.3687 ± 0.0024	75 ± 21	121 ± 5	-248 ± 2
NTH15PH60	0.0492 ± 0.0001	-0.0140 ± 0.0016	0.0068 ± 0.0015	0.3685 ± 0.0025	67 ± 21	126 ± 5	21 ± 1
NTH15PH90	0.0492 ± 0.0001	-0.0153 ± 0.0022	-0.0035 ± 0.0029	0.3690 ± 0.0021	60 ± 21	125 ± 4	286 ± 1
NTH15PH120	0.0493 ± 0.0001	-0.0126 ± 0.0022	-0.0129 ± 0.0037	0.3689 ± 0.0025	59 ± 21	117 ± 5	482 ± 2
NTH15PH150	0.0494 ± 0.0001	-0.0065 ± 0.0017	-0.0189 ± 0.0035	0.3692 ± 0.0023	68 ± 22	111 ± 5	546 ± 2
NTH30PH0	0.0481 ± 0.0001	-0.0040 ± 0.0021	0.0377 ± 0.0036	0.3588 ± 0.0028	129 ± 21	41 ± 6	-548 ± 3
NTH30PH30	0.0478 ± 0.0001	-0.0194 ± 0.0009	0.0285 ± 0.0003	0.3576 ± 0.0032	116 ± 19	71 ± 5	-58 ± 2
NTH30PH60	0.0477 ± 0.0001	-0.0288 ± 0.0015	0.0120 ± 0.0039	0.3575 ± 0.0035	85 ± 16	81 ± 6	417 ± 1
NTH30PH90	0.0480 ± 0.0001	-0.0324 ± 0.0013	-0.0075 ± 0.0060	0.3587 ± 0.0036	64 ± 16	61 ± 7	809 ± 2
NTH30PH120	0.0483 ± 0.0001	-0.0271 ± 0.0010	-0.0252 ± 0.0070	0.3602 ± 0.0031	74 ± 18	30 ± 8	1019 ± 3
NTH30PH150	0.0483 ± 0.0001	-0.0140 ± 0.0011	-0.0362 ± 0.0059	0.3601 ± 0.0029	108 ± 20	19 ± 8	927 ± 3
NTH45PH0	0.0456 ± 0.0001	-0.0075 ± 0.0041	0.0507 ± 0.0015	0.3410 ± 0.0039	103 ± 12	-6 ± 4	190 ± 1
NTH45PH10	0.0456 ± 0.0001	-0.0167 ± 0.0051	0.0481 ± 0.0000	0.3409 ± 0.0041	85 ± 11	10 ± 3	425 ± 1
NTH45PH20	0.0456 ± 0.0001	-0.0258 ± 0.0063	0.0445 ± 0.0010	0.3412 ± 0.0042	63 ± 10	19 ± 3	636 ± 1
NTH45PH30	0.0457 ± 0.0001	-0.0334 ± 0.0066	0.0395 ± 0.0021	0.3419 ± 0.0041	40 ± 10	20 ± 3	820 ± 1
NTH45PH40	0.0459 ± 0.0001	-0.0397 ± 0.0064	0.0331 ± 0.0031	0.3422 ± 0.0045	20 ± 8	16 ± 3	967 ± 1
NTH45PH45	0.0459 ± 0.0001	-0.0425 ± 0.0063	0.0297 ± 0.0035	0.3425 ± 0.0046	12 ± 8	12 ± 3	1026 ± 1
NTH45PH50	0.0460 ± 0.0001	-0.0455 ± 0.0068	0.0261 ± 0.0038	0.3426 ± 0.0049	3 ± 8	5 ± 3	1089 ± 1
NTH45PH60	0.0462 ± 0.0001	-0.0491 ± 0.0062	0.0177 ± 0.0049	0.3432 ± 0.0051	-9 ± 7	-10 ± 4	1191 ± 2
NTH45PH75	0.0464 ± 0.0001	-0.0535 ± 0.0069	0.0056 ± 0.0048	0.3445 ± 0.0049	-18 ± 7	-41 ± 4	1318 ± 3
NTH45PH90	0.0466 ± 0.0001	-0.0548 ± 0.0074	-0.0081 ± 0.0061	0.3455 ± 0.0045	-11 ± 8	-74 ± 4	1380 ± 3
NTH45PH975	0.0466 ± 0.0001	-0.0530 ± 0.0068	-0.0150 ± 0.0065	0.3453 ± 0.0048	-1 ± 7	-89 ± 6	1378 ± 3
NTH45PH120	0.0466 ± 0.0001	-0.0441 ± 0.0052	-0.0338 ± 0.0075	0.3452 ± 0.0043	47 ± 9	-111 ± 6	1217 ± 3
NTH45PH1125	0.0466 ± 0.0001	-0.0480 ± 0.0059	-0.0281 ± 0.0075	0.3454 ± 0.0045	29 ± 9	-108 ± 6	1297 ± 3
NTH45PH1275	0.0465 ± 0.0001	-0.0394 ± 0.0042	-0.0388 ± 0.0073	0.3448 ± 0.0042	65 ± 10	-110 ± 7	1114 ± 3
NTH45PH150	0.0460 ± 0.0001	-0.0211 ± 0.0003	-0.0494 ± 0.0058	0.3431 ± 0.0037	110 ± 12	-76 ± 6	633 ± 2
NTH60PH0	0.0440 ± 0.0001	-0.0101 ± 0.0070	0.0640 ± 0.0008	0.3260 ± 0.0042	-109 ± 4	121 ± 1	1435 ± 5
NTH60PH30	0.0444 ± 0.0001	-0.0449 ± 0.0119	0.0525 ± 0.0003	0.3271 ± 0.0048	-202 ± 2	46 ± 1	1568 ± 4
NTH60PH60	0.0443 ± 0.0001	-0.0674 ± 0.0138	0.0269 ± 0.0015	0.3275 ± 0.0044	-194 ± 3	-71 ± 3	1447 ± 3
NTH60PH90	0.0438 ± 0.0000	-0.0736 ± 0.0141	-0.0051 ± 0.0015	0.3263 ± 0.0036	-97 ± 3	-145 ± 3	1050 ± 2
NTH60PH120	0.0430 ± 0.0000	-0.0563 ± 0.0063	-0.0385 ± 0.0044	0.3233 ± 0.0035	25 ± 4	-96 ± 3	227 ± 1
NTH60PH150	0.0430 ± 0.0000	-0.0260 ± 0.0010	-0.0600 ± 0.0041	0.3231 ± 0.0039	26 ± 4	43 ± 3	-743 ± 3
NTH120PH0	0.0333 ± 0.0000	0.0040 ± 0.0049	0.0713 ± 0.0008	0.2683 ± 0.0012	-105 ± 1	48 ± 2	480 ± 3
NTH120PH30	0.0330 ± 0.0000	-0.0339 ± 0.0062	0.0659 ± 0.0018	0.2667 ± 0.0013	-43 ± 2	-117 ± 3	-101 ± 1
NTH120PH60	0.0332 ± 0.0000	-0.0617 ± 0.0040	0.0433 ± 0.0015	0.2678 ± 0.0014	108 ± 3	-145 ± 4	-516 ± 3
NTH120PH90	0.0335 ± 0.0001	-0.0748 ± 0.0021	0.0085 ± 0.0009	0.2710 ± 0.0005	229 ± 4	-40 ± 4	-835 ± 5
NTH120PH120	0.0340 ± 0.0001	-0.0668 ± 0.0007	-0.0289 ± 0.0005	0.2736 ± 0.0001	223 ± 3	147 ± 3	-1155 ± 5
NTH120PH150	0.0339 ± 0.0001	-0.0401 ± 0.0035	-0.0589 ± 0.0010	0.2719 ± 0.0006	26 ± 2	199 ± 2	-1008 ± 5
NTH135PH0	0.0315 ± 0.0000	0.0120 ± 0.0016	0.0597 ± 0.0008	0.2576 ± 0.0016	-103 ± 1	-105 ± 2	-670 ± 3
NTH135PH30	0.0318 ± 0.0000	-0.0204 ± 0.0033	0.0571 ± 0.0001	0.2582 ± 0.0021	21 ± 2	-122 ± 2	-898 ± 5
NTH135PH60	0.0318 ± 0.0000	-0.0464 ± 0.0031	0.0389 ± 0.0009	0.2582 ± 0.0025	95 ± 3	-36 ± 1	-915 ± 6
NTH135PH90	0.0317 ± 0.0000	-0.0594 ± 0.0017	0.0111 ± 0.0005	0.2575 ± 0.0031	66 ± 3	75 ± 1	-772 ± 6
NTH135PH120	0.0314 ± 0.0000	-0.0570 ± 0.0008	-0.0197 ± 0.0004	0.2562 ± 0.0025	-61 ± 1	120 ± 2	-370 ± 4
NTH135PH150	0.0313 ± 0.0000	-0.0402 ± 0.0001	-0.0455 ± 0.0008	0.2560 ± 0.0019	-154 ± 1	22 ± 1	210 ± 1
NTH165PH0	0.0292 ± 0.0001	0.0083 ± 0.0017	0.0220 ± 0.0008	0.2525 ± 0.0023	-98 ± 1	142 ± 3	-288 ± 2
NTH165PH30	0.0292 ± 0.0001	-0.0044 ± 0.0007	0.0212 ± 0.0005	0.2527 ± 0.0022	-82 ± 1	141 ± 3	-333 ± 2
NTH165PH60	0.0292 ± 0.0001	-0.0158 ± 0.0006	0.0146 ± 0.0016	0.2527 ± 0.0022	-75 ± 1	155 ± 3	-293 ± 2
NTH165PH90	0.0292 ± 0.0001	-0.0230 ± 0.0016	0.0041 ± 0.0025	0.2526 ± 0.0021	-84 ± 1	170 ± 3	-176 ± 1
NTH165PH120	0.0292 ± 0.0001	-0.0240 ± 0.0023	-0.0074 ± 0.0025	0.2523 ± 0.0023	-100 ± 1	171 ± 3	-8 ± 1
NTH165PH150	0.0292 ± 0.0001	-0.0187 ± 0.0023	-0.0169 ± 0.0019	0.2523 ± 0.0024	-107 ± 1	157 ± 3	164 ± 1

TABLE XVI: Radiated mass, angular momentum, and the remnant recoil (in original frame) as calculated from ψ_4. Errors quoted are from differences between to extrapolation to $r = \infty$. See Tables XVII and XVIII for more accurate measurement of the error.

CONF	$\delta M_{\rm rad}$	δJ_x	δJ_y	δJ_z	V_x	V_y	V_z
STH45PH0	0.0380 ± 0.0001	-0.0039 ± 0.0022	0.0033 ± 0.0029	0.3026 ± 0.0035	-61 ± 1	255 ± 3	783 ± 3
STH45PH30	0.0371 ± 0.0001	-0.0046 ± 0.0034	0.0018 ± 0.0009	0.2988 ± 0.0036	-14 ± 1	261 ± 2	-471 ± 3
STH45PH60	0.0371 ± 0.0001	-0.0047 ± 0.0043	0.0013 ± 0.0008	0.3000 ± 0.0032	-16 ± 2	265 ± 2	-1335 ± 6
STH45PH90	0.0376 ± 0.0001	-0.0035 ± 0.0040	0.0006 ± 0.0010	0.3036 ± 0.0025	-47 ± 3	265 ± 1	-1835 ± 8
STH45PH120	0.0384 ± 0.0001	-0.0003 ± 0.0017	-0.0016 ± 0.0011	0.3065 ± 0.0025	-70 ± 3	262 ± 1	-2004 ± 8
STH45PH150	0.0386 ± 0.0001	0.0028 ± 0.0009	-0.0032 ± 0.0030	0.3068 ± 0.0030	-89 ± 1	254 ± 2	-1707 ± 5
KTH45PH0	0.0389 ± 0.0001	-0.0026 ± 0.0029	0.1083 ± 0.0020	0.2797 ± 0.0025	147 ± 2	-486 ± 1	-1777 ± 4
KTH45PH30	0.0392 ± 0.0001	-0.0670 ± 0.0145	0.0932 ± 0.0006	0.2802 ± 0.0031	477 ± 2	-314 ± 2	-2022 ± 3
KTH45PH60	0.0394 ± 0.0001	-0.1143 ± 0.0243	0.0517 ± 0.0020	0.2809 ± 0.0043	578 ± 4	-7 ± 1	-2042 ± 5
KTH45PH90	0.0401 ± 0.0001	-0.1251 ± 0.0207	-0.0043 ± 0.0024	0.2841 ± 0.0053	469 ± 7	327 ± 2	-1991 ± 3
KTH45PH105	0.0408 ± 0.0001	-0.1166 ± 0.0157	-0.0336 ± 0.0030	0.2873 ± 0.0050	295 ± 5	447 ± 4	-1805 ± 2
KTH45PH120	0.0413 ± 0.0001	-0.1011 ± 0.0115	-0.0591 ± 0.0029	0.2892 ± 0.0048	63 ± 3	430 ± 5	-1355 ± 2
KTH45PH135	0.0412 ± 0.0001	-0.0809 ± 0.0087	-0.0795 ± 0.0028	0.2884 ± 0.0044	-134 ± 1	218 ± 3	-578 ± 1
KTH45PH150	0.0402 ± 0.0001	-0.0565 ± 0.0059	-0.0961 ± 0.0045	0.2835 ± 0.0047	-186 ± 1	-113 ± 2	411 ± 3
KTH45PH165	0.0392 ± 0.0001	-0.0290 ± 0.0024	-0.1062 ± 0.0045	0.2802 ± 0.0036	-64 ± 1	-387 ± 1	1280 ± 4
KTH22.5PH0	0.0385 ± 0.0001	-0.0025 ± 0.0038	0.0642 ± 0.0020	0.2929 ± 0.0038	266 ± 9	-43 ± 1	-1641 ± 4
KTH22.5PH30	0.0387 ± 0.0001	-0.0320 ± 0.0026	0.0537 ± 0.0015	0.2943 ± 0.0031	337 ± 9	130 ± 1	-1315 ± 6
KTH22.5PH60	0.0386 ± 0.0001	-0.0531 ± 0.0012	0.0285 ± 0.0047	0.2943 ± 0.0028	231 ± 9	296 ± 1	-793 ± 5
KTH22.5PH90	0.0380 ± 0.0001	-0.0604 ± 0.0001	-0.0030 ± 0.0058	0.2920 ± 0.0034	33 ± 8	315 ± 1	-23 ± 3
KTH22.5PH120	0.0375 ± 0.0001	-0.0511 ± 0.0017	-0.0348 ± 0.0070	0.2898 ± 0.0037	-71 ± 10	136 ± 1	948 ± 1
KTH22.5PH150	0.0378 ± 0.0001	-0.0278 ± 0.0039	-0.0567 ± 0.0050	0.2903 ± 0.0044	58 ± 9	-55 ± 1	1594 ± 2
LPH0	0.0538 ± 0.0002	-0.0085 ± 0.0084	0.0676 ± 0.0004	0.3813 ± 0.0071	74 ± 10	334 ± 6	2734 ± 3
LPH30	0.0544 ± 0.0002	-0.0460 ± 0.0141	0.0566 ± 0.0011	0.3834 ± 0.0068	-30 ± 7	246 ± 5	2181 ± 1
LPH60	0.0545 ± 0.0002	-0.0688 ± 0.0132	0.0312 ± 0.0024	0.3840 ± 0.0064	-51 ± 9	150 ± 5	1479 ± 1
LPH90	0.0538 ± 0.0002	-0.0765 ± 0.0123	-0.0050 ± 0.0053	0.3819 ± 0.0061	36 ± 14	95 ± 5	311 ± 3
LPH120	0.0524 ± 0.0002	-0.0639 ± 0.0083	-0.0371 ± 0.0033	0.3767 ± 0.0068	207 ± 14	169 ± 5	-1473 ± 3
LPH150	0.0525 ± 0.0002	-0.0327 ± 0.0004	-0.0614 ± 0.0021	0.3771 ± 0.0070	231 ± 13	341 ± 6	-2835 ± 1
N9TH55PH0	0.0453 ± 0.0001	-0.0099 ± 0.0057	0.0724 ± 0.0097	0.3334 ± 0.0057	59 ± 2	43 ± 3	499 ± 2
N9TH55PH30	0.0458 ± 0.0001	-0.0411 ± 0.0061	0.0550 ± 0.0025	0.3362 ± 0.0055	-49 ± 6	68 ± 3	1197 ± 1
N9TH55PH60	0.0465 ± 0.0001	-0.0641 ± 0.0079	0.0245 ± 0.0029	0.3395 ± 0.0055	-124 ± 8	4 ± 2	1592 ± 1
N9TH55PH90	0.0471 ± 0.0001	-0.0736 ± 0.0116	-0.0102 ± 0.0052	0.3422 ± 0.0052	-119 ± 4	-107 ± 3	1804 ± 4
N9TH55PH150	0.0458 ± 0.0001	-0.0275 ± 0.0003	-0.0633 ± 0.0066	0.3362 ± 0.0045	89 ± 1	-82 ± 3	594 ± 5

TABLE XVII: Comparison between remnant horizon properties and radiated quantities. Differences between the two is a much better measurement of the true error.

CONF	$\delta M_{\rm rad}$	$\delta M_{\rm rem}$	$\delta J_{x\rm rad}$	$\delta J_{x\rm rem}$	$\delta J_{y\rm rad}$	$\delta J_{y\rm rem}$	$\delta J_{z\rm rad}$	$\delta J_{z\rm rem}$
NTH15PH0	0.0494	0.0510	−0.0015	0.0059	0.0199	0.0301	0.3690	0.3774
NTH15PH30	0.0493	0.0509	−0.0090	−0.0178	0.0154	0.0132	0.3687	0.3774
NTH15PH60	0.0492	0.0508	−0.0140	−0.0266	0.0068	0.0065	0.3685	0.3770
NTH15PH90	0.0492	0.0508	−0.0153	−0.0284	−0.0035	−0.0037	0.3690	0.3770
NTH15PH120	0.0493	0.0509	−0.0126	−0.0228	−0.0129	−0.0142	0.3689	0.3773
NTH15PH150	0.0494	0.0510	−0.0065	0.0006	−0.0189	−0.0135	0.3692	0.3783
NTH30PH0	0.0481	0.0496	−0.0040	−0.0103	0.0377	0.0419	0.3588	0.3673
NTH30PH30	0.0478	0.0493	−0.0194	−0.0079	0.0285	0.0276	0.3576	0.3676
NTH30PH60	0.0477	0.0493	−0.0288	−0.0419	0.0120	0.0186	0.3575	0.3661
NTH30PH90	0.0480	0.0495	−0.0324	−0.0426	−0.0075	−0.0047	0.3587	0.3674
NTH30PH120	0.0483	0.0499	−0.0271	−0.0207	−0.0252	−0.0262	0.3602	0.3697
NTH30PH150	0.0483	0.0499	−0.0140	−0.0234	−0.0362	−0.0322	0.3601	0.3687
NTH45PH0	0.0456	0.0470	−0.0075	−0.0052	0.0507	0.0588	0.3410	0.3496
NTH45PH10	0.0456	0.0470	−0.0167	−0.0183	0.0481	0.0399	0.3409	0.3520
NTH45PH20	0.0456	0.0471	−0.0258	−0.0215	0.0445	0.0380	0.3412	0.3523
NTH45PH30	0.0457	0.0472	−0.0334	−0.0329	0.0395	0.0528	0.3419	0.3504
NTH45PH40	0.0459	0.0473	−0.0397	−0.0358	0.0331	0.0463	0.3422	0.3515
NTH45PH45	0.0459	0.0474	−0.0425	−0.0413	0.0297	0.0420	0.3425	0.3518
NTH45PH50	0.0460	0.0475	−0.0455	−0.0488	0.0261	0.0398	0.3426	0.3517
NTH45PH60	0.0462	0.0476	−0.0491	−0.0436	0.0177	0.0089	0.3432	0.3552
NTH45PH75	0.0464	0.0479	−0.0535	−0.0563	0.0056	0.0187	0.3445	0.3538
NTH45PH90	0.0466	0.0481	−0.0548	−0.0523	−0.0081	−0.0145	0.3455	0.3556
NTH45PH975	0.0466	0.0481	−0.0530	−0.0497	−0.0150	−0.0188	0.3453	0.3557
NTH45PH120	0.0466	0.0481	−0.0441	−0.0393	−0.0338	−0.0413	0.3452	0.3547
NTH45PH1125	0.0466	0.0481	−0.0480	−0.0455	−0.0281	−0.0317	0.3454	0.3551
NTH45PH1275	0.0465	0.0480	−0.0394	−0.0337	−0.0388	−0.0458	0.3448	0.3542
NTH45PH150	0.0460	0.0475	−0.0211	−0.0215	−0.0494	−0.0548	0.3431	0.3514
NTH60PH0	0.0440	0.0455	−0.0101	−0.0120	0.0640	0.0716	0.3260	0.3347
NTH60PH30	0.0444	0.0459	−0.0449	−0.0279	0.0525	0.0521	0.3271	0.3384
NTH60PH60	0.0443	0.0457	−0.0674	−0.0522	0.0269	0.0308	0.3275	0.3378
NTH60PH90	0.0438	0.0452	−0.0736	−0.0521	−0.0051	0.0000	0.3263	0.3372
NTH60PH120	0.0430	0.0443	−0.0563	−0.0613	−0.0385	−0.0366	0.3233	0.3305
NTH60PH150	0.0430	0.0444	−0.0260	−0.0362	−0.0600	−0.0527	0.3231	0.3319
NTH120PH0	0.0333	0.0343	0.0040	0.0197	0.0713	0.0722	0.2683	0.2732
NTH120PH30	0.0330	0.0340	−0.0339	−0.0382	0.0659	0.0635	0.2667	0.2718
NTH120PH60	0.0332	0.0341	−0.0617	−0.0512	0.0433	0.0453	0.2678	0.2745
NTH120PH90	0.0335	0.0344	−0.0748	−0.0675	0.0085	0.0101	0.2710	0.2762
NTH120PH120	0.0340	0.0350	−0.0668	−0.0788	−0.0289	−0.0384	0.2736	0.2748
NTH120PH150	0.0339	0.0349	−0.0401	−0.0412	−0.0589	−0.0565	0.2719	0.2763
NTH135PH0	0.0315	0.0325	0.0120	0.0112	0.0597	0.0560	0.2576	0.2634
NTH135PH30	0.0318	0.0327	−0.0204	−0.0187	0.0571	0.0564	0.2582	0.2646
NTH135PH60	0.0318	0.0327	−0.0464	−0.0410	0.0389	0.0341	0.2582	0.2657
NTH135PH90	0.0317	0.0326	−0.0594	−0.0615	0.0111	0.0206	0.2575	0.2639
NTH135PH120	0.0314	0.0323	−0.0570	−0.0665	−0.0197	−0.0092	0.2562	0.2622
NTH135PH150	0.0313	0.0322	−0.0402	−0.0370	−0.0455	−0.0386	0.2560	0.2627
NTH165PH0	0.0292	0.0301	0.0083	0.0143	0.0220	0.0291	0.2525	0.2576
NTH165PH30	0.0292	0.0301	−0.0044	−0.0107	0.0212	0.0183	0.2527	0.2579
NTH165PH60	0.0292	0.0301	−0.0158	−0.0211	0.0146	0.0116	0.2527	0.2577
NTH165PH90	0.0292	0.0300	−0.0230	−0.0130	0.0041	0.0093	0.2526	0.2583
NTH165PH120	0.0292	0.0300	−0.0240	−0.0176	−0.0074	0.0046	0.2523	0.2583
NTH165PH150	0.0292	0.0300	−0.0187	−0.0206	−0.0169	−0.0213	0.2523	0.2573

TABLE XVIII: Comparison between remnant horizon properties and radiated quantities. Differences between the two is a much better measurement of the true error.

CONF	$\delta M_{\rm rad}$	$\delta M_{\rm rem}$	$\delta J_{x\rm rad}$	$\delta J_{x\rm rem}$	$\delta J_{y\rm rad}$	$\delta J_{y\rm rem}$	$\delta J_{z\rm rad}$	$\delta J_{z\rm rem}$
STH45PH0	0.0380	0.0396	−0.0039	0.0029	0.0033	0.0113	0.3026	0.3100
STH45PH30	0.0371	0.0386	−0.0046	0.0049	0.0018	0.0106	0.2988	0.3066
STH45PH60	0.0371	0.0386	−0.0047	0.0060	0.0013	0.0059	0.3000	0.3071
STH45PH90	0.0376	0.0391	−0.0035	−0.0044	0.0006	−0.0119	0.3036	0.3097
STH45PH120	0.0384	0.0400	−0.0003	0.0021	−0.0016	0.0083	0.3065	0.3127
STH45PH150	0.0386	0.0403	0.0028	0.0007	−0.0032	−0.0130	0.3068	0.3134
KTH45PH0	0.0389	0.0407	−0.0026	−0.0097	0.1083	0.1226	0.2797	0.2830
KTH45PH30	0.0392	0.0410	−0.0670	−0.0624	0.0932	0.1065	0.2802	0.2851
KTH45PH60	0.0394	0.0410	−0.1143	−0.0927	0.0517	0.0556	0.2809	0.2912
KTH45PH90	0.0401	0.0417	−0.1251	−0.1215	−0.0043	0.0020	0.2841	0.2903
KTH45PH105	0.0408	0.0424	−0.1166	−0.1208	−0.0336	−0.0407	0.2873	0.2915
KTH45PH120	0.0413	0.0430	−0.1011	−0.0903	−0.0591	−0.0560	0.2892	0.2990
KTH45PH135	0.0412	0.0429	−0.0809	−0.0688	−0.0795	−0.0758	0.2884	0.2990
KTH45PH150	0.0402	0.0420	−0.0565	−0.0628	−0.0961	−0.0995	0.2835	0.2901
KTH45PH165	0.0392	0.0410	−0.0290	−0.0360	−0.1062	−0.1073	0.2802	0.2869
KTH22.5PH0	0.0385	0.0401	−0.0025	0.0103	0.0642	0.0695	0.2929	0.3018
KTH22.5PH30	0.0387	0.0403	−0.0320	−0.0232	0.0537	0.0594	0.2943	0.3036
KTH22.5PH60	0.0386	0.0402	−0.0531	−0.0497	0.0285	0.0387	0.2943	0.3030
KTH22.5PH90	0.0380	0.0396	−0.0604	−0.0621	−0.0030	0.0085	0.2920	0.3010
KTH22.5PH120	0.0375	0.0391	−0.0511	−0.0589	−0.0348	−0.0412	0.2898	0.2976
KTH22.5PH150	0.0378	0.0394	−0.0278	−0.0388	−0.0567	−0.0611	0.2903	0.2988
LPH0	0.0538	0.0562	−0.0085	0.0001	0.0676	0.0788	0.3813	0.3941
LPH30	0.0544	0.0568	−0.0460	−0.0336	0.0566	0.0663	0.3834	0.3969
LPH60	0.0545	0.0567	−0.0688	−0.0657	0.0312	0.0233	0.3840	0.3977
LPH90	0.0538	0.0560	−0.0765	−0.0650	−0.0050	0.0082	0.3819	0.3956
LPH120	0.0524	0.0546	−0.0639	−0.0494	−0.0371	−0.0439	0.3767	0.3906
LPH150	0.0525	0.0548	−0.0327	−0.0280	−0.0614	−0.0688	0.3771	0.3902
N9TH55PH0	0.0453	0.0468	−0.0099	−0.0033	0.0724	0.0536	0.3334	0.3461
N9TH55PH30	0.0458	0.0473	−0.0411	−0.0410	0.0550	0.0657	0.3362	0.3445
N9TH55PH60	0.0465	0.0479	−0.0641	−0.0599	0.0245	0.0161	0.3395	0.3509
N9TH55PH90	0.0471	0.0486	−0.0736	−0.0695	−0.0102	−0.0158	0.3422	0.3516
N9TH55PH150	0.0458	0.0473	−0.0275	−0.0266	−0.0633	−0.0531	0.3362	0.3466

TABLE XIX: BH spins during final plunge, recoil velocity, and the angle between $\vec{\Delta}_\perp$ for PHYYY and $\vec{\Delta}_\perp$ of the corresponding PH0 configuration; all calculated in a rotated frame where the infall occurs in the xy plane.

CONF	S_{x1}	S_{y1}	S_{z1}	S_{x2}	S_{y2}	S_{z2}	V_x	V_y	V_z	φ
NTH15PH0	0.0319	−0.0412	0.2000	0.0000	0.0000	0.0000	77	−110	−457	0
NTH15PH30	0.0454	−0.0238	0.1998	0.0000	0.0000	0.0000	79	−110	−252	24.5
NTH15PH60	0.0470	−0.0014	0.2012	0.0000	0.0000	0.0000	82	−117	15	50.5
NTH15PH90	0.0372	0.0210	0.2022	0.0000	0.0000	0.0000	85	−126	279	81.7
NTH15PH120	−0.0249	−0.0216	0.2030	0.0000	0.0000	0.0000	−116	−98	476	122.8
NTH15PH150	−0.0083	0.0475	0.2009	0.0000	0.0000	0.0000	79	−117	543	152.1
NTH30PH0	0.0818	−0.0569	0.1806	0.0000	0.0000	0.0000	62	−82	−555	0
NTH30PH30	0.0930	−0.0060	0.1840	0.0000	0.0000	0.0000	90	−94	−70	31.1
NTH30PH60	0.0761	0.0376	0.1876	0.0000	0.0000	0.0000	113	−111	403	61.1
NTH30PH90	0.0451	0.0711	0.1885	0.0000	0.0000	0.0000	111	−117	798	92.4
NTH30PH120	0.0058	0.0908	0.1853	0.0000	0.0000	0.0000	84	−108	1012	121.2
NTH30PH150	−0.0501	0.0865	0.1806	0.0000	0.0000	0.0000	66	−78	928	154.9
NTH45PH0	0.1277	0.0051	0.1612	0.0000	0.0000	0.0000	97	−86	173	0
NTH45PH10	0.1209	0.0302	0.1639	0.0000	0.0000	0.0000	111	−98	408	11.7
NTH45PH20	0.1136	0.0452	0.1658	0.0000	0.0000	0.0000	113	−112	619	19.4
NTH45PH30	0.0991	0.0710	0.1664	0.0000	0.0000	0.0000	128	−110	804	33.3
NTH45PH40	0.0891	0.0822	0.1666	0.0000	0.0000	0.0000	119	−115	954	40.4
NTH45PH45	0.0852	0.0866	0.1660	0.0000	0.0000	0.0000	119	−116	1012	43.2
NTH45PH50	0.0790	0.0932	0.1657	0.0000	0.0000	0.0000	116	−115	1077	47.4
NTH45PH60	0.0645	0.1057	0.1646	0.0000	0.0000	0.0000	110	−109	1181	56.3
NTH45PH75	0.0368	0.1220	0.1615	0.0000	0.0000	0.0000	100	−93	1311	70.9
NTH45PH90	0.0061	0.1328	0.1574	0.0000	0.0000	0.0000	82	−72	1377	85.1
NTH45PH975	−0.0093	0.1353	0.1552	0.0000	0.0000	0.0000	72	−62	1377	91.6
NTH45PH120	−0.0640	0.1261	0.1498	0.0000	0.0000	0.0000	47	−29	1222	114.6
NTH45PH1125	−0.0430	0.1331	0.1512	0.0000	0.0000	0.0000	52	−41	1300	105.6
NTH45PH1275	−0.0687	0.1234	0.1497	0.0000	0.0000	0.0000	38	−37	1120	116.8
NTH45PH150	−0.1109	0.0837	0.1516	0.0000	0.0000	0.0000	46	−44	644	140.7
NTH60PH0	0.0666	0.1442	0.1310	0.0000	0.0000	0.0000	103	−72	1439	0
NTH60PH30	−0.0104	0.1677	0.1188	0.0000	0.0000	0.0000	65	−11	1581	28.3
NTH60PH60	−0.0465	0.1658	0.1127	0.0000	0.0000	0.0000	35	6	1461	40.4
NTH60PH90	−0.1169	0.1294	0.1088	0.0000	0.0000	0.0000	17	33	1064	66.9
NTH60PH120	−0.1616	0.0407	0.1195	0.0000	0.0000	0.0000	54	−15	242	100.7
NTH60PH150	−0.1399	−0.0672	0.1345	0.0000	0.0000	0.0000	113	−85	−731	140.4
NTH120PH0	−0.1641	0.0877	−0.0856	0.0000	0.0000	0.0000	7	152	470	0
NTH120PH30	−0.1909	−0.0090	−0.0731	0.0000	0.0000	0.0000	27	104	−119	30.8
NTH120PH60	−0.1803	−0.0696	−0.0682	0.0000	0.0000	0.0000	47	77	−539	49.2
NTH120PH90	−0.1519	−0.1190	−0.0694	0.0000	0.0000	0.0000	54	71	−862	66.2
NTH120PH120	−0.0569	−0.1801	−0.0833	0.0000	0.0000	0.0000	38	113	−1179	100.6
NTH120PH150	0.0757	−0.1666	−0.0944	0.0000	0.0000	0.0000	4	168	−1014	142.6
NTH135PH0	−0.1314	−0.1005	−0.1230	0.0000	0.0000	0.0000	45	122	−673	0
NTH135PH30	−0.0650	−0.1461	−0.1307	0.0000	0.0000	0.0000	37	143	−894	28.6
NTH135PH60	0.0019	−0.1537	−0.1371	0.0000	0.0000	0.0000	25	169	−905	53.3
NTH135PH90	0.0664	−0.1355	−0.1383	0.0000	0.0000	0.0000	15	184	−757	78.7
NTH135PH120	0.1391	−0.0699	−0.1354	0.0000	0.0000	0.0000	12	174	−352	115.9
NTH135PH150	0.1620	0.0274	−0.1237	0.0000	0.0000	0.0000	30	138	221	152.2
NTH165PH0	−0.0416	−0.0470	−0.1949	0.0000	0.0000	0.0000	33	194	−272	0
NTH165PH30	−0.0132	−0.0579	−0.1992	0.0000	0.0000	0.0000	32	197	−313	28.7
NTH165PH60	0.0197	−0.0533	−0.1999	0.0000	0.0000	0.0000	29	200	−273	61.8
NTH165PH90	0.0419	−0.0385	−0.1993	0.0000	0.0000	0.0000	23	200	−162	89.
NTH165PH120	0.0625	−0.0059	−0.1992	0.0000	0.0000	0.0000	28	197	−3	126.2
NTH165PH150	−0.1161	0.0870	−0.1459	0.0000	0.0000	0.0000	−87	−126	199	153.2

TABLE XX: BH spins during final plunge, recoil velocity, and the angle between $\vec{\Delta}_\perp$ for PHYYY and $\vec{\Delta}_\perp$ of the corresponding PH0 configuration; all calculated in a rotated frame where the infall occurs in the xy plane.

CONF	S_{x1}	S_{y1}	S_{z1}	S_{x2}	S_{y2}	S_{z2}	V_x	V_y	V_z	φ
STHPH0	−0.1274	0.0542	0.1520	0.1323	−0.0633	−0.1432	78	−252	783	0
STHPH30	−0.1346	−0.0245	0.1531	0.1453	0.0137	−0.1435	43	−255	−472	33.4
STHPH60	−0.1086	−0.0869	0.1521	0.1205	0.0774	−0.1449	21	−258	−1336	61.7
STHPH90	−0.0518	−0.1308	0.1499	0.0642	0.1262	−0.1464	38	−258	−1836	91.4
STHPH120	0.0080	−0.1428	0.1486	−0.0002	0.1422	−0.1480	39	−262	−2005	116.3
STHPH150	0.0729	−0.1216	0.1493	−0.0707	0.1259	−0.1458	60	−260	−1707	144.
KTH45PH0	−0.1815	−0.0207	0.0933	−0.0487	0.1872	−0.0674	233	−379	−1794	0
KTH45PH30	−0.1429	−0.1005	0.1079	−0.1384	0.1353	−0.0637	331	−434	−2029	28.6
KTH45PH60	−0.1211	−0.1249	0.1099	−0.1619	0.1083	−0.0590	362	−421	−2048	39.4
KTH45PH90	−0.0720	−0.1559	0.1132	−0.1905	0.0554	−0.0447	354	−373	−2007	58.7
KTH45PH105	−0.0252	−0.1722	0.1101	−0.2015	0.0088	−0.0292	288	−316	−1833	75.1
KTH45PH120	0.0383	−0.1761	0.0998	−0.1966	−0.0540	−0.0165	201	−229	−1390	95.8
KTH45PH135	0.0954	−0.1604	0.0870	−0.1722	−0.1112	−0.0182	123	−166	−597	114.2
KTH45PH150	0.1499	−0.1161	0.0793	−0.1166	−0.1662	−0.0344	98	−177	419	135.7
KTH45PH165	0.1792	−0.0546	0.0833	−0.0413	−0.1939	−0.0553	133	−273	1304	156.5
KTH22.5PH0	−0.0319	−0.0997	0.1773	−0.1181	0.0640	−0.1535	183	−412	−1601	0
KTH22.5PH30	0.0234	−0.1086	0.1736	−0.1453	0.0117	−0.1429	157	−366	−1304	29.9
KTH22.5PH60	0.0671	−0.0983	0.1680	−0.1454	−0.0353	−0.1396	125	−321	−807	52.1
KTH22.5PH90	0.1000	−0.0737	0.1641	−0.1246	−0.0757	−0.1423	75	−304	−58	71.4
KTH22.5PH120	0.1216	−0.0141	0.1656	−0.0575	−0.1199	−0.1558	80	−339	895	101.6
KTH22.5PH150	0.0905	0.0627	0.1748	0.0521	−0.1121	−0.1631	158	−411	1534	142.5
LPH0	−0.1823	0.0481	0.0786	0.0331	−0.1292	0.1568	−449	196	2711	0
LPH30	−0.1783	−0.0098	0.0986	0.0830	−0.1177	0.1469	−271	108	2175	17.9
LPH60	−0.1634	−0.0601	0.1074	0.1181	−0.0968	0.1377	−156	60	1478	35.0
LPH90	−0.1337	−0.1136	0.1060	0.1453	−0.0628	0.1308	−99	55	307	55.2
LPH120	−0.0550	−0.1778	0.0877	0.1565	0.0119	0.1323	−154	166	−1480	87.6
LPH150	0.1125	−0.1602	0.0608	0.0802	0.1154	0.1508	−471	320	−2807	139.9
N9TH55PH0	0.1589	0.0385	0.1633	0.0000	0.0000	0.0000	123	−78	483	0
N9TH55PH30	0.1216	0.1024	0.1684	0.0000	0.0000	0.0000	145	−110	1186	26.5
N9TH55PH60	0.0759	0.1459	0.1641	0.0000	0.0000	0.0000	138	−88	1589	48.9
N9TH55PH90	0.0070	0.1746	0.1533	0.0000	0.0000	0.0000	96	−32	1808	74.1
N9TH55PH150	−0.1669	0.0663	0.1452	0.0000	0.0000	0.0000	37	22	604	144.7

TABLE XXI: Comparing the measured value of the z component of the recoil to values of $\Delta_\perp$, $S_\perp$, Δ_z, and S_z in a rotated frame where the infall occurs in the xy plane. These data are equivalent to the data given in Table XX.

CONF	$\Delta_\perp$	$S_\perp$	Δ_z	S_z	V_z	φ
STHPH0	0.554431	0.0100482	-0.574235	0.00849741	783	0
STHPH30	0.549469	0.014804	-0.577022	0.00931534	-472	33.4
STHPH60	0.548492	0.0148527	-0.577713	0.00691211	-1336	61.7
STHPH90	0.548418	0.0128664	-0.576338	0.0034721	-1836	91.4
STHPH120	0.554563	0.00763799	-0.576841	0.000557287	-2005	116.3
STHPH150	0.556667	0.00463136	-0.574073	0.00338651	-1707	144.
KTH45PH0	0.482864	0.278006	-0.314672	0.025327	-1794	0
KTH45PH30	0.461636	0.277368	-0.335907	0.0432341	-2029	28.6
KTH45PH60	0.463533	0.277454	-0.330673	0.0498387	-2048	39.4
KTH45PH90	0.474237	0.27512	-0.309072	0.0671106	-2007	58.7
KTH45PH105	0.49451	0.273523	-0.272672	0.0792363	-1833	75.1
KTH45PH120	0.518154	0.273345	-0.227693	0.081597	-1390	95.8
KTH45PH135	0.53259	0.276256	-0.205852	0.0673191	-597	114.2
KTH45PH150	0.530731	0.278283	-0.222612	0.0439408	419	135.7
KTH45PH165	0.510513	0.278202	-0.271257	0.0273344	1304	156.5
KTH22.5PH0	0.36197	0.150821	-0.647166	0.0233074	-1601	0
KTH22.5PH30	0.405488	0.152353	-0.619208	0.0300111	-1304	29.9
KTH22.5PH60	0.433706	0.151486	-0.602048	0.0277844	-807	52.1
KTH22.5PH90	0.439438	0.148127	-0.599516	0.0213135	-58	71.4
KTH22.5PH120	0.407051	0.14526	-0.62892	0.00966813	895	101.6
KTH22.5PH150	0.350353	0.147598	-0.661258	0.0114223	1534	142.5
LPH0	0.545401	0.166029	0.152806	0.230131	2711	0
LPH30	0.55264	0.155548	0.0943003	0.239985	2175	17.9
LPH60	0.554897	0.159654	0.059131	0.239545	1478	35.0
LPH90	0.554391	0.172777	0.0485684	0.23149	307	55.2
LPH120	0.555339	0.190078	0.0873465	0.215063	-1480	87.6
LPH150	0.542329	0.193387	0.175821	0.206818	-2807	139.9

[1] F. Pretorius, Phys. Rev. Lett. **95**, 121101 (2005), gr-qc/0507014.
[2] M. Campanelli, C. O. Lousto, P. Marronetti, and Y. Zlochower, Phys. Rev. Lett. **96**, 111101 (2006), gr-qc/0511048.
[3] J. G. Baker, J. Centrella, D.-I. Choi, M. Koppitz, and J. van Meter, Phys. Rev. Lett. **96**, 111102 (2006), gr-qc/0511103.
[4] M. Campanelli, C. O. Lousto, and Y. Zlochower, Phys. Rev. **D74**, 041501(R) (2006), gr-qc/0604012.
[5] M. Campanelli, C. O. Lousto, Y. Zlochower, and D. Merritt, Astrophys. J. **659**, L5 (2007), gr-qc/0701164.
[6] J. A. González, M. D. Hannam, U. Sperhake, B. Brugmann, and S. Husa, Phys. Rev. Lett. **98**, 231101 (2007), gr-qc/0702052.
[7] M. Campanelli, C. O. Lousto, Y. Zlochower, and D. Merritt, Phys. Rev. Lett. **98**, 231102 (2007), gr-qc/0702133.
[8] C. O. Lousto, H. Nakano, Y. Zlochower, and M. Campanelli, Phys. Rev. **D81**, 084023 (2010), 0910.3197.
[9] S. Komossa, H. Zhou, and H. Lu, Astrop. J. Letters **678**, L81 (2008), 0804.4585.
[10] G. A. Shields and E. W. Bonning, Astrophys. J. **682**, 758 (2008), 0802.3873.
[11] T. Bogdanovic, M. Eracleous, and S. Sigurdsson, Astrophys. J. **697**, 288 (2009), 0809.3262.
[12] F. Civano et al., Astrophys. J. **717**, 209 (2010), 1003.0020.
[13] M. Eracleous, T. A. Boroson, J. P. Halpern, and J. Liu, The Astrophysical Journal Supplement **201**, 23 (2012), 1106.2952.
[14] P. Tsalmantza, R. Decarli, M. Dotti, and D. W. Hogg, Astrophys. J. **738**, 20 (2011), 1106.1180.
[15] J. M. Comerford, R. L. Griffith, B. F. Gerke, M. C. Cooper, J. A. Newman, et al., Astrophys. J. **702**, L82 (2009), 0906.3517.
[16] F. Civano, M. Elvis, G. Lanzuisi, T. Aldcroft, M. Trichas, et al., Astrophys. J. **752**, 49 (2012), 1205.0815.
[17] L. Blecha, F. Civano, M. Elvis, and A. Loeb (2012), 1205.6202.
[18] S. Komossa, Adv. Astron. **2012**, 364973 (2012), 1202.1977.
[19] T. Bogdanovic, C. S. Reynolds, and M. C. Miller, Astrophys. J. **661**, L147 (2007), astro-ph/0703054.
[20] M. Dotti, M. Volonteri, A. Perego, M. Colpi, M. Ruszkowski, and F. Haardt, mnras **402**, 682 (2010), 0910.5729.
[21] C. O. Lousto and Y. Zlochower, Phys. Rev. Lett. **107**, 231102 (2011), 1108.2009.
[22] C. O. Lousto, Y. Zlochower, M. Dotti, and M. Volonteri, Phys. Rev. **D85**, 084015 (2012), 1201.1923.
[23] L. Rezzolla et al., Astrophys. J. **679**, 1422 (2008), arXiv:0708.3999 [gr-qc].
[24] C. O. Lousto and Y. Zlochower, Phys. Rev. **D83**, 024003 (2011), 1011.0593.
[25] L. E. Kidder, Phys. Rev. **D52**, 821 (1995), gr-qc/9506022.
[26] E. Racine, A. Buonanno, and L. E. Kidder, Phys. Rev. **D80**, 044010 (2009), 0812.4413.
[27] C. O. Lousto, M. Campanelli, Y. Zlochower, and H. Nakano, Class. Quant. Grav. **27**, 114006 (2010), 0904.3541.
[28] C. O. Lousto and Y. Zlochower, Phys. Rev. **D79**, 064018 (2009), 0805.0159.
[29] J. A. González, U. Sperhake, B. Brugmann, M. Hannam, and S. Husa, Phys. Rev. Lett. **98**, 091101 (2007), gr-qc/0610154.
[30] M. J. Fitchett, MNRAS **203**, 1049 (1983).
[31] Y. Zlochower, M. Campanelli, and C. O. Lousto, Class. Quant. Grav. **28**, 114015 (2011), 1011.2210.
[32] L. Boyle, M. Kesden, and S. Nissanke, Phys. Rev. Lett. **100**, 151101 (2008), 0709.0299.
[33] H. Nakano, M. Campanelli, C. O. Lousto, and Y. Zlochower, Class. Quant. Grav. **28**, 134005 (2011), 1011.2767.
[34] G. B. Arfken and H. J. Weber, *Mathematical methods for physicists 6th ed.* (2005).
[35] M. Ansorg, B. Brügmann, and W. Tichy, Phys. Rev. **D70**, 064011 (2004), gr-qc/0404056.
[36] S. Brandt and B. Brügmann, Phys. Rev. Lett. **78**, 3606 (1997), gr-qc/9703066.
[37] C. O. Lousto, H. Nakano, Y. Zlochower, B. C. Mundim, and M. Campanelli, Phys. Rev. **D85**, 124013 (2012), 1203.3223.
[38] Y. Zlochower, J. G. Baker, M. Campanelli, and C. O. Lousto, Phys. Rev. **D72**, 024021 (2005), gr-qc/0505055.
[39] P. Marronetti, W. Tichy, B. Brügmann, J. Gonzalez, and U. Sperhake, Phys. Rev. **D77**, 064010 (2008), 0709.2160.
[40] C. O. Lousto and Y. Zlochower, Phys. Rev. **D77**, 024034 (2008), 0711.1165.
[41] F. Loffler, J. Faber, E. Bentivegna, T. Bode, P. Diener, et al., Class. Quant. Grav. **29**, 115001 (2012), 1111.3344.
[42] Einstein Toolkit home page: `http://einsteintoolkit.org`.
[43] Cactus Computational Toolkit home page: `http://cactuscode.org`.
[44] E. Schnetter, S. H. Hawley, and I. Hawke, Class. Quant. Grav. **21**, 1465 (2004), gr-qc/0310042.
[45] M. Alcubierre, B. Brügmann, P. Diener, M. Koppitz, D. Pollney, E. Seidel, and R. Takahashi, Phys. Rev. **D67**, 084023 (2003), gr-qc/0206072.
[46] J. R. van Meter, J. G. Baker, M. Koppitz, and D.-I. Choi, Phys. Rev. **D73**, 124011 (2006), gr-qc/0605030.
[47] J. Thornburg, Class. Quant. Grav. **21**, 743 (2004), gr-qc/0306056.
[48] O. Dreyer, B. Krishnan, D. Shoemaker, and E. Schnetter, Phys. Rev. **D67**, 024018 (2003), gr-qc/0206008.
[49] M. Campanelli and C. O. Lousto, Phys. Rev. **D59**, 124022 (1999), gr-qc/9811019.
[50] C. O. Lousto and Y. Zlochower, Phys. Rev. **D76**, 041502(R) (2007), gr-qc/0703061.
[51] Q. Yu, Y. Lu, R. Mohayaee, and J. Colin, Astrophys. J. **738**, 92 (2011), 1105.1963.
[52] K. R. Stewart, J. S. Bullock, E. J. Barton, and R. H. Wechsler, Astrophys. J. **702**, 1005 (2009), 0811.1218.
[53] P. F. Hopkins, K. Bundy, D. Croton, L. Hernquist, D. Keres, et al., Astrophys. J. **715**, 202 (2010), 0906.5357.
[54] D. Gerosa, M. Kesden, E. Berti, R. O'Shaughnessy, and U. Sperhake (2013), 1302.4442.
[55] E. Berti, M. Kesden, and U. Sperhake, Phys.Rev. **D85**, 124049 (2012), 1203.2920.
[56] M. Kesden, U. Sperhake, and E. Berti, Astrophys. J. **715**,

1006 (2010), 1003.4993.
[57] M. Kesden, U. Sperhake, and E. Berti, Phys. Rev. **D81**, 084054 (2010), 1002.2643.
[58] J. D. Schnittman, Phys. Rev. **D70**, 124020 (2004), astro-ph/0409174.
[59] E. Barausse, V. Morozova, and L. Rezzolla, Astrophys. J. **758**, 63 (2012), 1206.3803.